Diagenetic smectite-to-illite transition in clay-rich sediments: A reappraisal of X-ray diffraction results using the multi-specimen method

Bruno Lanson, Boris A. Sakharov, Francis Claret, Victor A. Drits

HAL Id: insu-00404406
https://hal-insu.archives-ouvertes.fr/insu-00404406

Submitted on 16 Jul 2009

1   Diagenetic smectite-to-illite transition in clay-rich sediments:

2   A reappraisal of X-ray diffraction results using the multi-specimen method

3

4 Bruno Lanson[1]

5 Boris A. Sakharov[2]

6 Francis Claret[1,3]

7 Victor A. Drits[2]

8

9 1 Mineralogy & Environments Group, LGCA, Maison des Géosciences, BP53, Université

10   Joseph Fourier – CNRS, 38041 Grenoble Cedex 9, France

11 2 Geological Institute, Russian Academy of Sciences, 7 Pyzhevsky street, 119017

12   Moscow, Russia

13 3 BRGM, 3 av. Claude Guillemin, F-45060 Orléans cedex 2, France

14

15 [*]Corresponding author: bruno.lanson@obs.uf-grenoble.fr

16

17 Key words: Clay minerals, Clay diagenesis, Illite-smectite, Mixed-layering, interstratification,

18 XRD, Gulf Coast.

19   ABSTRACT.   Smectite illitization is a common mineralogical reaction occurring

20   during the burial diagenesis of clay-rich sediments and shales, and has thus attracted

21   sustained interest over the last fifty years. Prior studies have concluded that smectite

22   illitization proceeds through a steady set of homogeneous reactions involving

23   intermediate mixed layers of varying compositions. In these intermediate structures,

24   illite and smectite, or, more generally, expandable layers (I and Exp layers, respectively)

25   coexist among the same crystallites giving rise to non-periodic structures (I-Exp)

26   characterized by specific diffraction effects. Consistent with this model, reaction

27   progress was characterized by the simultaneous increase in the illite content in I-Exp

28   and in their stacking order leading to the following mineralogical sequence: smectite →

29   randomly interstratified I-Exp with high smectite contents (> 50% Exp layers) →

30   ordered I-Exp with high illite contents (> 50% I layers) → illite. Although reaction

31   mechanisms have been extensively debated, this structural characterization has not been

32   challenged, possibly due to a methodological bias. In the present study, X-ray diffraction

33   patterns typical of the diagenetic illitization of smectite are interpreted using modern

34   approaches involving profile fitting (multi-specimen method). Novel insights into the

35   structure of intermediate reaction products are thus obtained. In particular, original

36   clay parageneses are described including the systematic presence of illite, kaolinite,

37   chlorite and a mixed layer containing kaolinite and expandable layers (K-Exp).

38   In contrast to previous descriptions, the early stages of smectite illitization are

39   characterized by the coexistence of discrete smectite and of a randomly interstratified I-

40   Exp with a high content of illite layers (>50% I layers). Both the smectite and the I-Exp

41   are authigenic and form under shallow burial, that is at low temperature conditions.

42   With increasing burial depth, the relative proportion of I-Exp increases, essentially at

43   the expense of discrete smectite, and the composition of I-Exp becomes slightly more

44   illitic. In the second stage of smectite illitization, two illite-containing mixed layers are

45   observed. They result from two parallel reaction mechanisms affecting the randomly

46   interstratified I-Exp present in the shallow section of the series. The first reaction

47   implies the dissolution of this randomly interstratified I-Exp and leads to the

48   crystallization of an ordered I-Exp without significant illitization, possibly because of the

49   low K-availability. The second reaction affecting the randomly interstratified I-Exp

50   implies the growth of trioctahedral (Mg, Al) hydroxide sheets in Exp interlayers, thus

51   developing di-trioctahedral chlorite layers (Ch layers) in the initial I-Exp to form an I-

52   Exp-Ch. A layer-by-layer mechanism is hypothesized for this reaction. In this scheme,

53   Mg cations released by the dissolution-recrystallization reaction of I-Exp likely

54   represent the source of Mg for the formation of brucite-like sheets in expandable

55   interlayers, and thus of the I-Exp-Ch.

56   The reported structural characterization of smectite illitization intermediate products

57   contradicts the conventional wisdom of a homogeneous reaction through a series of pure

58   mixed layers of variable composition. In contrast, the coexistence of different phases

59   implies a heterogeneous reaction via a sequence of intermediate phases and requires

60   reassessing the reaction mechanisms proposed in the literature. The compositional range

61   (relative proportion of the different layer types) of these phases is limited and smectite

62   illitization proceeds essentially as relative proportions of the different phases vary. In

63   addition, reaction kinetics and stability of the different intermediate products also need

64   to be reconsidered.

INTRODUCTION

66

67   For about half a century, smectite illitization has been extensively described in different

68   geological contexts: burial diagenesis of clay-rich sediments (Burst, 1957,1969; Weaver,

69   1957, 1959; Perry and Hower, 1970; Hower and others, 1976; Srodon, 1978, 1984a; Boles

70   and Francks, 1979; Velde and others, 1986; among many others), hydrothermal alteration of

71   volcanic tuffs (Inoue and others, 1978, 1988, 2005; Inoue and Utada, 1983; Altaner and

72   others, 2003), metasomatic alteration of bentonites (Hoffman and Hower, 1979; Velde and

73   Brusewitz, 1982, 1986; Inoue and others, 1990; Sucha and others, 1993; Li and others, 1997),

74   and contact metamorphism (Nadeau and Reynolds, 1981; Pytte and Reynolds, 1989; Drits and

75   others, 2007). Although different reaction mechanisms have been inferred (see Altaner and

76   Ylagan, 1997, for a review; Srodon and others, 2000), this mineralogical transition has been

77   systematically described to occur through mixed layers. In these intermediate structures, illite

78   and smectite, or more generally expandable, layers (I and Exp layers, respectively) coexist

79   among the same crystallites giving rise to non-periodic structures, hereafter referred to as I-

80   Exp. The structural characterization of I-Exp, essential for the reconstruction of thermal and

81   chemical paleoconditions, requires determining the nature of interstratified layers, their

82   relative proportions and their stacking sequences through analysis of their specific diffraction

83   effects (see Reynolds, 1980, Drits and Tchoubar, 1990, Moore and Reynolds, 1997, for

84   details). Such analysis has revealed that smectite illitization is a continuous two-stage reaction

85   characterized by a steady increase of the illite content in I-Exp and by the simultaneous

86   increase of stacking order: illite and expandable layers are interstratified at random when

87   expandable layers dominate ("R0 zone" – early diagenesis), whereas interstratification is

88   ordered when illite prevails ("R ≥ 1 zone" – late-stage diagenesis; Shutov and others, 1969;

89   Perry and Hower, 1970, 1972; Hower and others, 1976; Bethke and others, 1986; Srodon,

90   1999).

91   Following these pioneering works, simplified methods have been proposed for the

92   structural characterization of I-Exp from X-ray diffraction (XRD) data (Srodon, 1980, 1981,

93   1984b; Watanabe, 1981, 1988; Velde and others, 1986; Inoue and others, 1989; Moore and

94   Reynolds, 1997). These methods essentially rely on peak migration curves which link the

95   position of a given reflection (or of a set of reflections) to the composition (relative proportion

96   of the different layer types) of the mixed layers and to their stacking order. Peak migration

97   curves were obtained mostly from XRD patterns calculated using programs implemented

98   from Reynolds (1967, 1980) or Watanabe (1981) algorithms. These calculations were

99   essentially restricted to I-Exp composition and ordering that were described in the early works

100   reported above, thus confining the simplified identification methods to these specific mixed

101   layers. Logically, the early description of smectite illitization was not challenged by the

102   numerous subsequent case studies. The lack of direct comparison between experimental and

103   calculated XRD patterns concealed possible incomplete or erroneous identifications. A

104   significant proportion of the studies devoted to smectite illitization thus focused on the

105   definition of reaction mechanisms and on the possible use of this mineralogical

106   transformation as a paleogeothermometer. For the latter purpose, the influence of time and

107   temperature (Hower and others, 1976; Velde and Vasseur, 1992), K availability (Huang,

108   1993; Bauer and Velde, 1999), and water/rock ratio (Whitney, 1990) on reaction progress was

109   estimated.

110   However, a more appropriate crystallography-based approach has been developed over

111   the last decade. In particular, direct comparison between calculated and experimental

112   diffraction patterns has been favored and has allowed reproduction of not only the positions of

113   the reflections but also of their profiles, both of which are strongly influenced by

114   interstratification. In addition to the frequent occurrence of multi-component mixed layers in

115   nature, the multi-specimen method proposed initially by Drits and others (1997), and by

116   Sakharov and others (1999a, 1999b) uncovered the existence of mixed layers exhibiting

117   "unusual" composition and/or stacking order (Drits and others, 1997, 2002a, 2002b, 2004,

118   2007; Sakharov and others, 1999b, 2004; Lindgreen and others, 2000, 2002; Claret and

119   others, 2004; McCarty and others, 2004). This new approach thus challenges the commonly

120   accepted description of smectite illitization in diagenetic series by invalidating hypotheses

121   sustaining usual I-Exp identification criteria such as homogeneity of the swelling behavior,

122   random interstratification restricted to smectite-dominated mixed layers, absence of

123   segregation and of partial ordering, et cetera (see Lanson, 2005, for further discussion).

124   The present study thus aims at obtaining an accurate structural characterization of

125   samples characteristic of diagenetic smectite illitization in clay-rich sediments from modeling

126   of their XRD patterns. The proposed models are shown to be consistent with the coexistence

127   of discrete smectite with I-Exp, as has been observed on similar samples with transmission

128   electron microscopy. In addition, the definition of structure models at various stages of the

129   reaction constrains the possible reaction mechanisms of this transformation. In particular,

130   analysis of stacking parameters refutes the solid-state transformation hypothesis for illitization

131   of I-Exp over the "R0 zone", and for the transition from randomly interstratified I-Exp to

132   ordered varieties, consistent with crystal growth features reported during smectite illitization.

133   It is shown also that part of the I-Exp formed early in the "R0 zone" transforms, possibly

134   through solid-state processes, into a complex mixed layer present in the deeper samples.

135

MATERIALS AND METHODS

137

138 *Samples*

139   Samples were collected in two different onshore wells in the Texas Gulf Coast (Carter –

140 Tyler County in central Gulf Coast Texas, and Mustang Island – Nueces County in south Gulf

141 Coast Texas). These wells have been described previously by Velde and Espitalié (1989), and

142 Velde and Vasseur (1992), and the stratigraphic age of the samples ranges from Cretaceous to

143 Eocene (Carter well) and from Eocene to Pleistocene (Mustang Island). In the two wells, little

144 or no erosion has occurred and present depths are approximately maximum burial depths. The

145 temperature gradient is similar in both wells (32.7°C/km and 35°C/km, in Mustang Island and

146 Carter, respectively), and they both extend through most of the smectite-to-illite transition

147 (fig. 1).

148

149 *Experimental*

150   Carbonates were removed from all samples using the acetic acid-acetate buffer method

151 described in Moore and Reynolds (1997). Then, organic matter was removed at 50°C by

152 adding small aliquots of hydrogen peroxide ($H_2O_2 - 30\%$) to the suspension until gaseous

153 emission ceased. The <2 μm size fraction was extracted by centrifugation for a set of samples

154 selected from -2170 to -5500 m in Carter and Mustang Island boreholes. From preliminary

155 XRD results, 6 of the initial samples were selected as representative of the complete transition

156 between "smectite-rich" and "illite-rich" samples in Gulf Coast series. All samples were

157 selected in the Carter well at 2170, 3660, 4000, 4640, 5010, and 5180 m (samples A-F).

158   To minimize the contributions from mica, kaolinite, chlorite and quartz, the <0.2 μm

159 size fraction was extracted for these 6 samples. This fraction was then Ca-saturated.

160 Suspensions were kept in contact with a 1M $CaCl_2$ solution for 4-12 hours at room

161 temperature to ensure a complete cation exchange. After three replications of this procedure,

162 the excess chloride was rinsed with distilled water (Milli-Q – 18.2 MΩ.cm^{-1}).

163   Oriented preparations were obtained by pipetting a slurry of the Ca-saturated

164 suspensions on a glass side and drying this suspension at 40°C for a few hours to obtain an

165 air-dried (AD) preparation. Ethylene-glycol (EG) solvation of the slides was achieved by

166 exposing them to EG vapor at 70°C for a minimum of 12 hours. XRD patterns were recorded

167 with a Bruker D5000 powder diffractometer equipped with a Kevex Si(Li) solid state detector

168 using CuKα_{1+2} radiation. Intensities were recorded at 0.04° 2θ step intervals from 2 to 50°,

169 using a 6 sec counting time per step except for sample D (40 sec/step). Sizes of the divergence

170 slit, the two Soller slits, the antiscatter, and resolution slits were 0.5°, 2.3°, 2.3°, 0.5° and

171 0.06°, respectively. Humidity was controlled at 40% RH for AD measurements.

172

173 *XRD Profile Modeling*

174   Structure models were determined using the multi-specimen method described by Drits

175 and others (1997), and Sakharov and others (1999a, 1999b). In contrast to usual identification

176 methods of mixed layers, the multi-specimen method requires recording XRD patterns after

177 different treatments for each sample. For a given sample, these patterns usually differ

178 significantly because of the contrasting hydration/expansion behavior of expandable

179 interlayers in response to these treatments. The method itself relies on the direct comparison

180 of experimental profiles with those calculated for a structure model, the optimum agreement

181 between data and calculated patterns being obtained by a trial-and-error procedure.

182   The different treatments can affect the thickness and scattering power (nature, amount,

183 and position of interlayer species) of the expandable interlayers, but not the layer sequences

184 within the crystallites. As a consequence, a consistent structure model is obtained for a given

185 mixed layer when layer sequences obtained from all experimental profiles of a given sample

186   are nearly identical. XRD pattern modeling provides also a quantitative phase analysis of the

187   samples. One essential requirement for structure model soundness is that the relative weight

188   contributions of periodic and interstratified phases to the different XRD patterns of a given

189   sample must be similar (Sakharov and others, 1999b; Claret, 2001; Lindgreen and others,

190   2002; McCarty and others, 2004, 2005).

191   Structure models for each mixed layer include the number of the different layer types

192   (not limited to 2), their nature and relative proportions. Markovian statistics are used to

193   describe possible layer stacking sequences and the relative abundance thereof. An important

194   parameter of this statistical description is the Reichweit parameter R (Jagodzinski, 1949)

195   which characterizes the extent of ordering as the number of adjacent layers influencing the

196   nature of a given layer. For $R = 0$, layer types are thus randomly interstratified, whereas for

197    $R = 1$ the occurrence probability of a given layer type depends on the nature of its nearest

198   predecessor. For a given value of the R parameter, a set of probability parameters is needed to

199   completely describe layer stacking. The relative content of the different layer types (W_i) is

200   systematically needed together with junction probability parameters (P_{ij}). P_{ij} parameters

201   define the probability for a j-type layer to follow an i-type layer (i,j = I or Exp for I-Exp). W_i

202   and P_{ij} parameters are related, and only two parameters are necessary to describe a two-

203   component mixed layer with $R = 1$, W_I and P_{ExpExp} being commonly used for I-Exp. In this

204   case, specific layer stacking modes for $R = 1$ include maximum possible degree of ordering

205   (MPDO), which is obtained when pairs of the least abundant layers are prohibited in the

206   stacking, that is when $P_{ExpExp} = 0$ assuming $W_I > W_{Exp}$. Random interstratification occurs

207   when $P_{ExpExp} = P_{IExp} = W_{Exp} = 1 - W_I$, and physical mixture of I and Exp layers when $P_{ExpExp} =$

208   1 whatever the W_{Exp} value. In addition, a tendency to segregation of i-type layers is

209   characterized by $W_i < P_{ii}$ (i = I, Exp), whereas partial ordering occurs when $W_{Exp} > P_{ExpExp} > 0$

210   assuming $W_I > W_{Exp}$ (see Bethke and Altaner, 1986, Drits and Tchoubar, 1990, and Moore

211   and Reynolds, 1997, for details).

212   The algorithm developed initially by Drits and Sakharov (1976) and used recently by

213   Drits and others (1997) and Sakharov and others (1999b) was used to fit experimental XRD

214   profiles over the 2–50° 2θ range. Instrumental and experimental factors such as horizontal

215   and vertical beam divergences, goniometer radius, length and thickness of the oriented slides

216   were measured and introduced without further adjustment. Sigmastar (see Reynolds, 1986, for

217   details) was set to 12 and the mass absorption coefficient (μ^*) to 45, as recommended by

218   Moore and Reynolds (1997). In the profile fitting process, it was necessary to define different

219   types of Exp layers as a function of their hydration or swelling behavior in AD and EG states,

220   respectively (Drits and others, 2002a). Irrespective of the hydration/swelling behavior of Exp

221   layers, the relative contents of I and Exp layers and their stacking sequences should be the

222   same in both AD and EG states. The hydration/swelling behavior of Exp layers is likely

223   related to the amount and location of the layer charge deficit, although this behavior may

224   differ for a given layer from AD to EG states. In the following I, K, Ch, and Exp denote illite,

225   kaolinite, di-trioctahedral chlorite, and expandable layers, respectively. For all layer types z

226   atomic coordinates proposed by Moore and Reynolds (1997) were used after modification to

227   fit the layer thickness values used for simulation; thermal motion parameters (B) were also set

228   as proposed by Moore and Reynolds (1997). The position and amount of interlayer species

229   (H_2O and EG molecules in particular) were considered as variable parameters and varied

230   about the values proposed by Moore and Reynolds (1997) during the fitting process. In bi-

231   hydrated Exp layers (2W), a single plane of H_2O molecules was assumed to be present on

232   each side of the interlayer mid-plane as proposed by Ferrage and others (2005a, 2005b).

233   Finally, distributions of coherent scattering domain sizes (CSDSs) were assumed to be

234   lognormal and characterized by their mean value (Drits and others, 1997b). Quality of fit was

10

235 assessed over the 4-50°2θ (22.0-1.85 Å) range with the R_{wp} and R_{exp} factors (Howard and

236 Preston, 1989).

237

238   RESULTS

239

240   *Qualitative Description of the Experimental XRD Patterns.*

241   Evolution of sample structure with depth is best seen on XRD patterns obtained after

242 EG solvation (fig. 2A). The XRD pattern of sample A (2170 m) exhibits a strong peak at

243 ~16.9 Å, well resolved on its low-angle side, and weaker peaks at 8.6, 5.54, 3.331, 2.781, and

244 2.023 Å that form a non-rational series. In addition, peaks at 7.21, 3.58 and 2.38 Å and weak

245 modulations at ~10.0 and 5.0 Å correspond to finely dispersed kaolinite and to discrete illite,

246 respectively. The peak at ~17.0 Å is still intense for sample B (3660 m) but its resolution is

247 significantly reduced on its low-angle side. Compared to sample A, the reflections at 5.54 Å

248 and 2.781 Å are shifted to higher and lower angles, respectively, in the XRD pattern of

249 sample B. The reflection at 8.6 Å (sample A) is shifted also to lower angles and appears as a

250 high-angle shoulder of the 10.0 Å reflection (sample B). XRD patterns of samples B and C

251 are alike, except that the low-angle resolution of the ~17.0 Å peak is reduced for sample C

252 compared to sample B. Samples B and C also contain significant amounts of discrete illite and

253 kaolinite, and a small amount of chlorite.

254   XRD patterns of samples taken from depths > 4500 m (D, E, and F) are all akin and

255 their profiles strongly differ from those of samples A, B and C. Over the low-angle region,

256 there is no peak at ~17.0 Å, but broad maxima between ~13.5-15.0 Å (fig. 2). These patterns

257 also contain a super-reflection at ~30 Å, best seen for sample E, and additional broad maxima

258 at ~9.25-9.30 Å, and 5.20-5.25 Å. The low resolution of the latter reflections results to some

11

259 extent from their partial overlap with illite peaks at 10.0 Å and 5.0 Å. Finally, sharp kaolinite

260 and chlorite reflections are visible at 3.579 Å and 3.528 Å.

261 To summarize the above observations, the six samples can be divided in two groups.

262 XRD patterns of group I (samples A, B, and C) exhibit a ~17.0 Å reflection (EG state) whose

263 low-angle resolution decreases with increasing depth. XRD patterns of group II (samples D,

264 E, and F) exhibit a broad maximum at ~13.5-15.0 Å and a super-reflection at ~30 Å. XRD

265 patterns collected in AD conditions are shown in the Appendix (fig. A-1).

266 The described evolution of XRD patterns with depth is typical for smectite illitization

267 resulting from the burial diagenesis of clay-rich rocks. For example, XRD patterns presented

268 by Perry and Hower (1970) for samples E-2131 m, E-2554 m, and E-2667 m are almost

269 superimposed (except for the kaolinite reflections) to those of samples A, B and C,

270 respectively (fig. 3). Similarly, the XRD pattern presented by Perry and Hower (1970) for

271 sample E-3658 m resembles that of samples D and E, except for the low-angle intensity.

272 According to Hower and others (1976) the observed evolution is evidence for a continuous

273 smectite-to-illite reaction series occurring through intermediate mixed layers. However in

274 both the Perry and Hower (1970) and Hower and others (1976) studies, XRD pattern

275 interpretation was restricted to a qualitative comparison with patterns calculated for two-

276 component I-Exp (EG) models. The relative proportions of I and Exp layer types (W_i), and

277 their ordering (P_{ij} parameters) were the two essential parameters refined.

278

279   *Quantitative Description of Experimental XRD Profiles*

280 *Group I samples: single-phase segregated I-Exp model.*– According to this model, the

281 non-rational series of basal reflections corresponds to a unique I-Exp in which I and Exp

282 layers tend to segregate. XRD data are compared to calculated patterns in figure 4. Structural

283 parameters used to calculate these patterns are listed in tables 1 and 2. Along with the main I-

284   Exp contribution, samples contain kaolinite, illite (an illite-rich mixed layer with ~ 5% of

285   expandable layers), minor chlorite, and a randomly interstratified K-Exp containing 75%

286   kaolinite and 25% expandable layers. Although K-Exp have attracted considerably less

287   attention than I-Exp, natural K-Exp covering the whole compositional range have been

288   reported in the literature (see for example Sakharov and Drits, 1973; Sudo and Shimoda,

289   1977; Brindley and others, 1983). Consistent with these reports, K-Exp whose composition is

290   dominated by kaolinite layers exhibit broad diffraction maxima shifted from the ideal

291   kaolinite maxima towards the nearest smectite peaks as predicted by Méring (1949).

292   Transition from sample A to sample C corresponds to an increase in illite and K-Exp

293   content (from 5 to ~21%, and from 5 to ~15%, respectively – table 2) and to a decrease of I-

294   Exp (from 79 to ~53%). The kaolinite and chlorite content is about constant. With increasing

295   depth, I-Exp expandability decreases from 55% in sample A to 35% in samples B and C

296   (table 1A). Under AD conditions, three types of expandable layers (15.0, 12.5 and 14.0 Å

297   layers) are found in I-Exp from sample A, whereas only 2W and 1W layers (15.0 and 12.5 Å,

298   respectively) are encountered in samples B and C. After EG solvation all Exp layers in I-Exp

299   from sample A swell to 16.76 Å with two planes of EG molecules in their interlayers (2EG

300   layers). Swelling behavior is more heterogeneous in samples B and C (table 1A). In all three

301   samples, $W_I < P_{II}$ (table 1B) for I-Exp and illite layers are thus slightly segregated, as

302   estimated by the S_q parameter (Drits and Tchoubar, 1990):

303

304                    $S_q = (P_{ii} - W_i)/(1 - W_i)$ (1)

305

306   To determine S_q, it is convenient to use P_{II} and W_I values so as to disregard the actual

307   distribution of Exp layers. With increasing depth, the S_q parameter decreases from 0.27 to

308   0.19 and 0.10 (samples A, B and C, respectively), indicating that interstratification of I and

309   Exp layers tends to become random with increasing burial depth and illite content (table 1A).

310   The CSDS of I-Exp increases with burial depth from 7 (sample A) to 15 layers (samples B

311   and C – table 1A). For a given sample, the P_{ij} parameters refined for the I-Exp are different

312   for AD and EG states (table 1B). This apparent inconsistency arises from the contrasting

313   expansion behavior of Exp layers in AD and EG states, and vanishes if the hydration/swelling

314   behavior of Exp layers is carefully analyzed (see Appendix for details).

315   *Single-phase segregated I-Exp model: Intrinsic inconsistency of the model.*– If I-Exp in

316   group I samples represent a series of diagenetically altered mixed layers, the occurrence

317   probabilities of I and Exp layers, and those of the different layer pairs and triplets (W_i, W_{ij} =

318    $W_i \times P_{ij}$ and $W_{ijk} = W_i \times P_{ij} \times P_{jk}$, respectively – table 3) should evolve logically in the context

319   of illitization. For the sake of simplicity, all expandable layers will be considered together in

320   the following discussion. From these occurrence probabilities, transition from sample A to

321   sample B appears logical as the illite enrichment (from 45% to 65% at 2170 and 3660 m,

322   respectively) is associated with the decrease of occurrence probability for layer pairs, and

323   layer triplets (not shown), containing Exp layers (table 3). At the same time, the segregation

324   degree in I-Exp decreases from 0.27 (sample A) to 0.19 (sample B) because ExpExp pairs

325   disappear faster than II pairs form [$(W_{ExpExp})_B - (W_{ExpExp})_A$ = -0.205, and $(W_{II})_B - (W_{II})_A$ =

326   0.194 – table 3].

327   In the general illitization scheme, the steady evolution of a segregated I-Exp towards

328   random interstratification is a priori consistent with a solid-state transformation. The observed

329   decrease of the S_q parameter between samples B (0.19) and C (0.10) follows the same logic

330   although illite contents are similar in the two samples (table 3). However, when looking at the

331   different W_{ij} probabilities, the I-Exp evolution between samples B and C cannot be

332   interpreted reasonably in the illitization context. This evolution implies indeed the formation

333   of IExp and ExpI pairs at the expense of both II and ExpExp pairs [$(W_{II})_B > (W_{II})_C$ – table 3].

334   The single-phase segregated I-Exp model is thus inadequate to describe the structural

335   evolution of group I samples, and should be rejected.

336   *Group I samples: The mixture model.*– According to this model, the ~17 Å peak of

337   group I samples corresponds to discrete smectite coexisting with a randomly interstratified I-

338   Exp with a high content of illite layers (W_I > 50% – Claret, 2001; Drits and others, 2002b;

339   Claret and others, 2004; Lanson and others, 2005; McCarty, 2005; Aplin and others, 2006;

340   McCarty and others, 2008). Data are compared in figure 5 to XRD patterns calculated for this

341   model. Table 4A contains the structural and probability parameters for the I-Exp contribution,

342   whereas relative proportions of the different contributions to the diffraction patterns are

343   reported in table 5. In all group I samples, the major contribution is I-Exp whose relative

344   proportion increases with increasing burial depth from 44% to 50% and 57% (samples A, B

345   and C, respectively). Simultaneously, the content of discrete smectite decreases dramatically

346   from 27% to 5% and ~2% in samples A, B and C, respectively. As for the single-phase

347   segregated I-Exp model the content of discrete illite increases significantly with depth from

348   5% to ~17% and 21% in samples A, B and C. I-Exp is randomly interstratified despite its high

349   illite content that ranges from 57% to 62 and 67% (samples A, B and C, respectively). I-Exp

350   has the same mean (12 layers) and maximum (50 layers) CSDS in all group I samples (table

351   4A). A randomly interstratified K-Exp with 75% kaolinite layers completes the clay

352   paragenesis. K-Exp exhibits broad diffraction maxima at ~6.8-7.0 and 3.4-3.5 Å both in AD

353   state and after EG solvation (fig. A-2A, B).

354   *Group II samples.*– Along with 4-5% of chlorite, 5-10% of illite (with 5% Exp layers),

355   6-12% of kaolinite, all group II samples contain I-Exp, I-Exp-Ch and K-Exp mixed layers.

356   The structural and probability parameters providing the best fit to XRD data (fig. 5) are

357   reported in table 4C. The major phases are I-Exp and I-Exp-Ch. The relative proportion of I-

358   Exp decreases slightly with burial depth from 40% (sample D) to 33 and 34% (samples E and

359   F, respectively) whereas that of I-Exp-Ch steadily increases from 27% to 31% and 42%

360   (samples D, E and F, respectively).

361   Parallel to this phase composition change, transition from sample D to sample F is

362   characterized by a slight increase of the illite content in I-Exp (from 70 to 75%). In sample D,

363   interstratification of I and Exp layers is ordered (R = 1) with MPDO ($P_{Exp1Exp1} = P_{Exp1Exp2} =$

364    $P_{Exp2Exp1} = P_{Exp2Exp2} = 0$). Longer-range ordering (R = 2 – table 4C) is observed for samples E

365   and F. In the latter samples P_{ij} parameters are similar to sample D, and longer-range ordering

366   is characterized by a slight segregation of IExpIExp sequences as $P_{ExpIExp} > W_{Exp} / W_I$ (see

367   Drits and Tchoubar, 1990, for details). Compared to I-Exp in group I samples, the size of I-

368   Exp CSDs is significantly increased for group II samples (mean and maximum values are 15

369   and 100 layers compared to 12 and 50, respectively, for group I samples – tables 4A, 4C). In

370   all group II samples, I-Exp-Ch contains 70% of illite layers interstratified with Exp and di-

371   trioctahedral chlorite layers, the proportion of Ch layers increasing from 15% in samples D

372   and E, to 20% in sample F. In contrast to the ordered I-Exp, I-Exp-Ch CSDSs are similar to

373   those determined for the I-Exp in group I samples (tables 4A, 4C). Finally, K-Exp (R = 0)

374   consists of 75% kaolinite and 25% Exp layers as in group I samples.

375

376   DISCUSSION

377

378   *Reliability of Structure Models*

379   The results obtained in the present work demonstrate the ability of the multi-specimen

380   approach to provide good quality fit to experimental data obtained on natural polyphasic

381   samples, in agreement with previous studies (Drits and others, 1997a, 2002a, 2002b, 2004;

382   Sakharov and others, 1999a, 1999b; Lindgreen and others, 2000, 2002; Claret and others,

383   2004; McCarty and others, 2004, 2008). This approach can thus be used to determine accurate

384   structural parameters for the phases present in a given sample. In the present work,

385   satisfactory fit to experimental positions, intensities and profiles of basal XRD reflections was

386   obtained using up to three mixed layers, each incorporating from two to four layer types, in

387   addition to discrete phases.

388   Obviously, the more discrete and mixed-layer phases that coexist in a sample, the more

389   independent structural parameters that are needed for simulation. As a result, the reliability

390   and accuracy in determining these parameters may decrease as more phases are introduced,

391   although constraints are provided by the required uniqueness of structure models used to fit

392   different patterns of a given sample (AD and EG patterns of Ca-saturated samples in the

393   present case).

394   *Evidence for the actual phase composition.–* As the optimum fits to XRD data were

395   obtained using a trial-and-error approach, the actual sensitivity of XRD simulations to key

396   structural parameters needs to be assessed. The presence of the different contributions is the

397   first of these parameters, and samples B and E will be used as typical for group I and II,

398   respectively. Elementary contributions to the intensity diffracted by these two samples are

399   shown in the Appendix (fig. A-2, A-3). Figure 6 compares the XRD pattern of sample B with

400   those calculated for models similar to the optimal one (fig. 5) after subtraction of the

401   contributions of discrete smectite or of K-Exp. Logically, the absence of the minor smectite

402   contribution leads to the absence of the 17 Å peak in the calculated EG pattern (fig. 6A – R_{wp}

403   = 17.56%). Similarly, the absence of the K-Exp contribution leads to significant misfits at

404   ~11.5^o and ~26°2θ (fig. 6B – R_{wp} = 16.00%).

405   For group II samples, exclusion of either I-Exp or I-Exp-Ch contributions in the

406   calculated XRD pattern decreases dramatically the agreement with the data. For example,

407   calculated intensity is reduced in the low-angle region if the I-Exp contribution is subtracted

408   from the optimal fit (fig. 7A). Additional significant misfits are observed at 16-19° 2θ and 26-

409   36° 2θ in both EG and AD XRD patterns (fig. 7A – R_{wp} = 23.04%, and fig. 7B – R_{wp} =

410   27.73%, respectively). Figure 7C (R_{wp} = 20.62%) shows that the I-Exp-Ch contribution is

411   essential to fit the AD pattern in the 18-20 and 26-31° 2θ ranges. In the present work, mixed

412   layers are introduced only if they allowed fitting specific angular ranges without significant

413   overlap with other phases.

414   *Evidence for the presence of chlorite layers in I-Exp-Ch.–* The actual nature of the

415   mixed layer coexisting with the ordered I-Exp was determined after testing numerous illite-

416   containing structure models with contrasting amounts, and distributions, of Exp layers: in

417   addition to I and Exp layers the optimum mixed layer (I-Exp-Ch) contains di-trioctahedral

418   layers consisting of dioctahedral 2:1 layers and of trioctahedral brucite-like interlayer sheets.

419   Despite a similar basal spacing, the 14.0 Å Ch layers can be differentiated from 14.0 Å Exp

420   layers because of their contrasting scattering factors. If Ch layers (with 3.0 Mg and 6.0 OH

421   per half unit-cell in their interlayers) are replaced by Exp layers (with 0.25 Mg and 2.0 H_2O

422   per half unit-cell in their interlayers), significant misfits are visible at 17-18° and 26-31° 2θ

423   for sample E (fig. 8A – R_{wp} = 17.41%). XRD patterns calculated for the optimum I-Exp-Ch

424   contribution and for the contribution in which Ch layers are replaced by Exp layers are shown

425   in figure A-4. The strong intensity increase at 17-18° 2θ induced by the presence of Ch layers

426   is related to the specific intensity distribution observed for sudoite (di-trioctahedral chlorite),

427   whose 4.7 Å reflection is most intense (Lin and Bailey, 1985; Billault and others, 2002;

428   Kameda and others, 2007).

429   *Heterogeneous hydration/swelling of Exp layers.–* In both AD and EG states, Exp layers

430   present in mixed layers often exhibit various interlayer configurations and *d*-spacings as

431   reported for reference smectite samples (Ferrage and others, 2005b, 2007). For example, in

432   the AD state I-Exp from group I samples systematically contains 15.0, 14.0 and 12.5 Å layers

433   (table 4). Sensitivity of XRD to such heterogeneous behavior may be assessed by replacing,

434   for example, 14.0 Å Exp layers (8% of the layers in I-Exp from sample B) either by 15.0 Å or

435   by 12.5 Å layers (fig. 8B and C, respectively). In both cases, significant misfits are visible at

436   28-30° 2θ.

437

438   *Diagenetic Illitization of Clay-rich Sediments: A Two-Stage Process*

439   Undoubtedly, illitization of clay-rich sediments during burial diagenesis of mudstones

440   and shales ranks among the most important and most documented mineral reactions. In the

441   present work, the innovative interpretation of XRD patterns provides detailed information on

442   the different phases present in the sediments and on their evolution. As a result, a structural

443   mechanism can be proposed which contrasts with the usual description of a continuous

444   transformation described by Perry and Hower (1970), Hower and others (1976) and many

445   other authors (see Srodon, 1999, for a review). According to this commonly accepted model,

446   diagenetic illitization of clay-rich sediments consists of two main stages whose existence is

447   not challenged in the present study. The evolution of the mineralogical composition, and the

448   structural evolution of individual phases will thus be described separately for group I and

449   group II samples.

450   *Smectite illitization in the upper part of the series (group I samples).*– The commonly

451   accepted model assumes the steady illitization of a unique randomly interstratified I-Exp. By

452   contrast two phases, a discrete smectite and a randomly interstratified I-Exp with high illite

453   content, coexist in group I samples in addition to discrete illite, kaolinite, K-Exp and chlorite

454   (except for sample A). When burial depth increases the relative proportion of discrete

455   smectite decreases sharply from 27% at 2170 m to 2-3% at 4000 m and the illite content in I-

456   Exp increases (from 57% to 67% at the same depths). Except for a few early reports (Perry

457   and Hower, 1970, 1972; Reynolds and Hower, 1970; Bethke and others, 1986), randomly

458   interstratified I-Exp with such high illite contents have seldom been described in diagenetic

459 environments, interstratification of I and Exp layers being usually described as ordered (R = 1

460 and MPDO) when illite layers prevail. However, the coexistence of discrete smectite with

461 randomly interstratified I-Exp with high illite content is possibly widespread at shallow depth

462 in sedimentary basins, the absence of significant maximum in the low-angle region being

463 responsible for their scarce description. The steady decrease of the 17.0 Å peak intensity and

464 of its low-angle resolution observed with depth for group I samples is indeed characteristic of

465 the early stage of the diagenetic smectite-to-illite transition (fig. 3).

466 A similar mineralogical composition was described in the Callovo-Oxfordian

467 sedimentary formation (Paris Basin – Claret, 2001; Claret and others, 2004). Using the same

468 methodological approach McCarty (2005), and McCarty and others (2008) also demonstrated

469 that discrete smectite and randomly interstratified I-Exp with high illite content coexist in

470 shallow samples from the off-shore Gulf Coast. The similarities between the XRD patterns

471 recorded for group I samples and those obtained from Gulf Coast wells B and E by Perry and

472 Hower (1970, 1972) support such a coexistence in the latter samples. TEM observations

473 performed on shallow samples from various sedimentary basins also support the ubiquity of

474 such a clay paragenesis (Dong and others, 1997; Dong, 2005; Freed and Peacor, 1992).

475 I-Exp in group I samples are characterized also by heterogeneous hydration/swelling

476 behavior of Exp layers. In the AD state, 1W ($d_{001} \sim 12.5$ Å) and 2W ($d_{001} \sim 15.0$ Å) layers

477 systematically coexist in I-Exp (table 4), most likely as a consequence of the heterogeneous

478 distribution of the amount and/or location of the layer-charge deficit. However, layer-charge

479 heterogeneity is likely not considerable as both layer types swell to 16.7-16.9 Å following EG

480 solvation (table 4). In addition, I-Exp includes 14.0 Å layers present in similar proportions

481 under AD and EG conditions. These layers cannot be considered as smectite layers as their

482 basal spacing remains constant upon EG solvation, and their actual nature is unclear. Their

483 basal spacing and swelling behavior are consistent with hydroxy-interlayered vermiculite

20

484   layers that are often found in soils as a separate phase (Douglas, 1989; Moore and Reynolds,

485   1997; Chen and others, 2001; Marques and others, 2002). The observed hydration/swelling

486   heterogeneity of Exp layers is most likely common in natural samples, thus impairing the

487   potential of most usual identification methods for I-Exp as discussed in more detail by

488   McCarty and others (2008).

489   *Group I samples: origin of the randomly interstratified I-Exp with high illite content*

490   *(~65%I).–* It is commonly assumed that the smectite-to-illite reaction starts from a pure

491   smectite precursor. However, Hower and others (1976) pointed out that in young sedimentary

492   basins the pure smectite stage may be concealed by the high variability of smectite contents in

493   randomly interstratified I-Exp from surface samples. According to Jennings and Thompson

494   (1986) and Velde and Vasseur (1992), the compositional homogenization of I-Exp, likely

495   through its recrystallization and formation of pure smectite, occurs at burial depths ranging

496   typically from several hundred meters in older rocks to 1-2 km in younger ones. Smectite then

497   acts as a precursor for the diagenetic smectite-to-illite conversion (Velde and Iijima, 1988). In

498   the Carter well, the presence of pure smectite was inferred at 683 m from XRD analysis

499   (Berger and others, 1999). In the present study, no XRD data were collected over the 683-

500   2150 m depth interval. It is however reasonable to assume that steady smectite-to-illite

501   conversion occurs over this depth interval, and that both smectite and I-Exp are authigenic in

502   group I samples. Additional support for the authigenic origin of I-Exp comes from the similar

503   XRD patterns obtained in this study and from other Gulf Coast samples (Perry and Hower,

504   1970, 1972). The diagenetic smectite-to-illite sequences described by the latter authors start

505   from very smectitic material and subsequently evolve to form parageneses having XRD

506   patterns very similar to those of group I samples (fig. 3).

507   *Group I samples: new description of smectite illitization during the first stage.–* From

508   the present interpretation of XRD patterns, the shallow part of the diagenetic smectite-to-illite

509   sequence thus corresponds to the formation of a randomly interstratified I-Exp with prevailing

510   illite layers ($W_I > 50\%$) at the expense of smectite which is present as a pure phase in the

511   shallowest samples. At burial depths lower than 4000 m, the overall smectite-to-illite

512   conversion thus results i) from the dissolution of pure smectite, and ii) from the formation of

513   the randomly interstratified I-Exp with $W_I > W_{Exp}$. The latter process is likely fed by smectite

514   dissolution and favored by K-availability. The overall (I-Exp + smectite) content decreases

515   with increasing burial depth (from ~70% in sample A to ~60% in sample C) possibly because

516   smectite dissolution does not only feed I-Exp formation. Several important conclusions derive

517   from these results.

518   The first stage of smectite illitization is heterogeneous, with the simultaneous progress

519   of smectite dissolution and of I-Exp illitization, in agreement with electron microscopy

520   observation of Gulf Coast shales (Dong and others, 1997; Dong, 2005; Freed and Peacor,

521   1992). As a consequence, pure smectite is present at significant burial depth, indicating a

522   much higher stability than commonly accepted. In the Carter well for example, pure smectite

523   which accounts for most of the clay fraction at 683 m (Berger and others, 1999) persists down

524   to ~4000 m depth where it still represents 2% of the clay fraction (table 5). Although in the

525   investigated samples smectite illitization proceeds simultaneously with partial smectite

526   dissolution, the two reactions do not appear to be systematically linked. For example, Claret

527   and others (2004) presented evidence that I-Exp composition is constant while smectite is

528   steadily dissolving over a narrow depth interval in the Callovo-Oxfordian formation (eastern

529   Paris basin). Similarly, McCarty (2005) and McCarty and others (2008) describe important

530   variations of discrete smectite relative proportion without any compositional evolution of the

531   coexisting I-Exp.

532   The new description also raises the need to reconsider the kinetics of smectite

533   illitization. According to the usual identification criteria (for example Srodon, 1981; Inoue

534 and others, 1989), XRD data obtained from the Carter samples correspond to an I-Exp with ~

535 20% illite layers (R = 0) down to ~2000 m depth (Velde and Vasseur, 1992; Berger and

536 others, 1999). Similarly, shallow samples from Gulf Coast wells are dominated by randomly

537 interstratified I-Exp with ~25% illite layers according to Perry and Hower (sample E-1829 m

538 - 1970, 1972). By contrast, XRD profile modeling shows that I-Exp contains 57% illite layers

539 at similar depth (sample A). Illitization is thus faster than commonly assumed as randomly

540 interstratified I-Exp with $W_I > W_{Exp}$ likely forms under shallow burial conditions consistent

541 with the TEM observations of Freed and Peacor (1992). The formation of a randomly

542 interstratified I-Exp having a given composition thus occurs at much lower temperature than

543 assumed from the commonly accepted model of smectite illitization for similar conditions of

544 burial diagenesis (temperature, pressure, K activity, water-rock ratio, et cetera). The illite

545 content in I-Exp obtained from both approaches may however be partially reconciled by

546 taking into account the contribution of pure smectite. When this contribution is minimum (2%

547 – sample C), similar compositions are determined for I-Exp (~65%I) using either the usual

548 identification criteria (3500-4000 m deep samples in Carter well, fig. 1 – Velde and Vasseur,

549 1992; Berger and others, 1999) or the present modeling approach.

550   In any case, the rate of smectite illitization strongly decreases with increasing burial

551 depth, in contrast with the commonly accepted model (see for example Srodon and Eberl,

552 1984). According to the present data, the illite content in I-Exp increases at a minimum rate of

553 40%I/km from 683 to 2170 m depth. By contrast, from 2170 m to 4000 m the increase of illite

554 content in I-Exp is limited to ~10% (table 4), at a rate of ~5%I/km. In agreement with Berger

555 and others (1999), this rate decrease is likely due to the low amount of available K, in relation

556 with the dissolution of K-feldspars and micas. In the studied samples, the maximum

557 illitization rate coincides with the dissolution of K-feldspars which disappear at ~2000 m in

558 the Carter well (Berger and others, 1999).

559   *Structural evolution of clay minerals during deep burial diagenesis (group II samples).*–

560   The presence of a unique illite-rich ordered (R ≥ 1) I-Exp is characteristic of deep burial

561   diagenesis in the commonly accepted model for smectite illitization. According to the present

562   modeling results, such a phase is actually present in group II samples coexisting with another

563   illite-containing mixed layer. In addition to illite and Exp layers, the latter structure includes

564   di-trioctahedral chlorite layers, whose formation is consistent with the low K-availability

565   (Whitney and Northrop, 1988) and whose relative proportion increases slightly with

566   increasing burial depth (table 4). Interstratification of the different layer types is almost

567   random in I-Exp-Ch, with only a slight tendency to segregation of Ch layers. By contrast, the

568   slight increase of the illite content in I-Exp is associated with a steady increase of layer

569   ordering. Specifically, the succession of dominant illite layers is favored and the extent of this

570   ordering (quantified by the Reichweit R parameter – Jagodzinski, 1949; Reynolds, 1980)

571   tends to increase beyond the nearest neighbor with increasing burial depth (table 4).

572   *Transition from group I to group II samples: structural evolution of I-Exp from group I*

573   *to group II samples.*– The illite content in I-Exp increases only slightly from sample C to

574   sample D, whereas the layer distribution is dramatically modified between the two samples,

575   interstratification being random in sample C and ordered (R =1 with MPDO) in sample D. In

576   the context of smectite illitization, II pairs should be preserved and solid-state transformation

577   can be hypothesized only if the relative proportion of IExp and ExpI pairs increases at the

578   expense of the sole ExpExp pairs. On the contrary, it is clear from table 6 that ExpExp pairs

579   originally present in sample C are not abundant enough (0.109) to account for the increase of

580   IExp and ExpI pairs from sample C to sample D $[(W_{IExp} + W_{ExpI})_D - (W_{IExp} + W_{ExpI})_C =$

581   0.158]. The transition from sample C to sample D can thus only result from a dissolution-

582   recrystallization process. Indirect support for the proposed mechanism comes from the

583   extremely low intensity scattered by sample D which required a seven-fold increase of the

584 collection time to obtain a similar signal-to-noise ratio for a given amount of material. The

585 low amplitude of the XRD signal is likely due to the presence of XRD-amorphous material

586 whose presence is expected for a major dissolution-reprecipitation process. Additional

587 indirect support arises from the significant CSDS increase observed for the I-Exp from

588 sample C to sample D (table 5). No K-Ar ages are available for the samples investigated in

589 the present study. However, Aronson and Hower (1976) reported significantly younger ages

590 for deep Gulf Coast samples (typical of group II samples) than for shallower samples (typical

591 of group I samples). The gap between the two groups of samples also supports a major

592 dissolution-recrystallization process leading to the crystallization of an ordered I-Exp at the

593 expense of a randomly interstratified I-Exp of similar composition.

594   *Transition from group I to group II samples: possible solid-state formation of I-Exp-Ch*

595 *at the expense of I-Exp.–* The illite contents in I-Exp from sample C and in I-Exp-Ch from

596 sample D are similar (67 and 70%I, respectively). Their junction probability parameters

597 exhibit also strong similarities, interstratification being random in I-Exp from sample C, and

598 showing only slight tendency to segregation in I-Exp-Ch from sample D (table 4C). In

599 addition, I-Exp from sample C and I-Exp-Ch from sample D have similar CSDSs. It is thus

600 possible to hypothesize a solid-state mechanism, involving Mg polymerization in former Exp

601 interlayers, for the transition between the two mixed layers. In this case, a series of mixed

602 layers with compositions intermediate between those of the two end members can be

603 envisaged. In I-Exp from sample C and in I-Exp-Ch from sample D, Exp layers are randomly

604 distributed within crystallites ($P_{Expi} = W_i$), whereas I and Ch layers are slightly segregated in

605 sample D ($W_I < P_{II}$, and $W_{Ch} < P_{ChCh}$). The degree of segregation of I and Ch layers in I-Exp-

606 Ch from sample D is 0.083 and 0.135, respectively (Eq. 1 – table 4C). To propose

607 compositional and structural parameters for intermediate phases, one may thus hypothesize

608 that the increase of I and Ch contents from sample C to sample D is accompanied by the

609   increase of their tendency to segregation. Probability parameters describing such theoretical

610   intermediate phases (phases I and II) are reported in table 7. In particular, the relative

611   proportions of I and Ch layers in these phases are equal to 68% and 5% (phase I) and 69%

612   and 10% (phase II), respectively, to account for the compositional change from sample C

613   (67%I and 0%Ch) to sample D (70%I and 15%Ch). In addition, the degrees of segregation of

614   I and Ch layers increase steadily from sample C (0.000 and 0.000, random interstratification)

615   to phase I (0.027 and 0.045), to phase II (0.054 and 0.090), and finally to sample D (0.083 and

616   0.135, respectively). Exp layers are randomly distributed in both intermediate phases so that

617    $P_{ExpExp} = W_{Exp}$, $P_{ExpI} = W_I$ and $P_{ExpCh} = W_{Ch}$ as in I-Exp from sample C and in I-Exp-Ch from

618   sample D. Possible mechanisms of the hypothesized solid-state transformation of I-Exp from

619   sample C to I-Exp-Ch from sample D through intermediate I-Exp-Ch phases are detailed in

620   the Appendix.

621

622   CONCLUDINGS REMARKS

623

624   *A General Pattern for Diagenetic Smectite-to-Illite Transition in Shales*

625   The XRD patterns obtained from the Carter well samples are typical for the diagenetic

626   smectite-to-illite transition (fig. 3). The multi-specimen method led however to an unusual

627   description of the data. In particular, an original clay paragenesis is reported and a novel

628   diagenetic evolution of this paragenesis proposed which includes two stages of smectite

629   illitization.

630   In the first stage, the clay paragenesis corresponds to the physical mixture of discrete

631   smectite and of a randomly interstratified I-Exp with a high content of illite layers ($W_I > 50\%$)

632   in addition to illite, kaolinite, chlorite and K-Exp. With increasing burial depth, the relative

633   proportion of I-Exp increases, essentially at the expense of discrete smectite, and its

634   composition becomes slightly more illitic. Several conclusions in this study contradict the

635   conventional wisdom of smectite-to-illite transition:

636   - Smectite illitization is a heterogeneous reaction involving the physical mixture of pure

637   smectite and I-Exp.

638   - Discrete smectite and I-Exp are authigenic.

639   - The apparent stability of smectite is higher than commonly assumed as this mineral persists

640   down to 4000 m, although its relative abundance decreases with increasing depth.

641   - Smectite illitization occurs very early and randomly interstratified I-Exp with $W_I > W_{Exp}$ is

642   formed at shallow burial depth, the temperature at which a I-Exp with a given composition is

643   formed being lower than commonly assumed.

644   - Smectite illitization rate decreases rapidly, most likely as the result of K-feldspar

645   dissolution.

646   In the second stage of smectite illitization (below 4000 m depth in the present case

647   study), clay paragenesis consists of two illite-containing mixed layers in addition to illite,

648   kaolinite, chlorite and K-Exp. These two illite-containing mixed layers result from two

649   parallel reaction mechanisms affecting the randomly interstratified I-Exp present in the upper

650   part of the series. The first reaction implies the dissolution of the I-Exp and the crystallization

651   of an ordered I-Exp with R = 1 (MPDO) without significant increase of the I layer content

652   (70% versus 67%, tables 4A, 4C), possibly as the result of low K-availability. With increasing

653   depth, ordering increases together with a marginal increase of the I layer content (up to 75%

654   in sample F – table 4C). The second reaction affects the remaining fraction of the randomly

655   interstratified I-Exp and implies the polymerization and growth of trioctahedral brucite-like

656   sheets in Exp interlayers, thus developing di-trioctahedral chlorite layers in the initial I-Exp to

657   form an I-Exp-Ch. A possible layer-by-layer mechanism is supported for this reaction by the

658   random layer distribution in the I-Exp-Ch, similar to that of the initial I-Exp. In this scheme,

659 Mg cations released by the dissolution-recrystallization of I-Exp likely represent the Mg

660 source for the formation of brucite-like sheets.

661

662

672

673 **REFERENCES**

674

675 Altaner, S. P., and Ylagan, R. F., 1997, Comparison of structural models of mixed-layer

676   illite/smectite and reaction mechanisms of smectite illitization: Clays & Clay

677   Minerals, v. 45, p. 517-533.

678 Altaner, S. P., Ylagan, R. F., Savin, S. M., Aronson, J. L., Belkin, H. E., and Pozzuoli, A.,

679   2003, Geothermometry, geochronology, and mass transfer associated with

680   hydrothermal alteration of a rhyolitic hyaloclastite from Ponza Island, Italy:

681   Geochimica Et Cosmochimica Acta, v. 67, p. 275-288.

682 Aplin, A. C., Matenaar, I. F., McCarty, D. K., and van Der Pluijm, B. A., 2006, Influence of

683   mechanical compaction and clay mineral diagenesis on the microfabric and pore-scale

684   properties of deep-water Gulf of Mexico Mudstones.: Clays & Clay Minerals, v. 54, p.

685   500-514.

686 Aronson, J. L., and Hower, J., 1976, The mechanism of burial metamorphism of argillaceous

687   sediments: 2. radiogenic argon evidence: Geological Society of America Bulletin, v.

688   87, p. 738-744.

689 Bauer, A., and Velde, B., 1999, Smectite transformation in high molar KOH solutions: Clay

690   Minerals, v. 34, p. 259-273.

691 Berger, G., Velde, B., and Aigouy, T., 1999, Potassium sources and illitization in Texas Gulf

692   Coast shale diagenesis: Journal of Sedimentary Research, v. 69, p. 151-157.

693 Bethke, C. G., and Altaner, S. P., 1986, Layer-by-layer mechanism of smectite illitization and

694   application to a new rate law: Clays & Clay Minerals, v. 34, p. 136-145.

695 Bethke, C. G., Vergo, N., and Altaner, S. P., 1986, Pathways of smectite illitization: Clays &

696   Clay Minerals, v. 34, p. 125-135.

697 Billault, V., Beaufort, D., Patrier, P., and Petit, S., 2002, Crystal-chemistry of Fe-sudoites

698   from Uranium deposits in the Athabasca basin (Saskatchewan, Canada): Clays & Clay

699   Minerals, v. 50, p. 70-81.

700 Boles, J. R., and Francks, G. S., 1979, Clay diagenesis in Wilcox sandstones of Southwest

701   Texas: Implications of smectite diagenesis on sandstone cementation: Journal of

702   Sedimentary Petrology, v. 49, p. 55-70.

703 Brindley, G. W., Suzuki, T., and Thiry, M., 1983, Interstratified kaolinite/smectites from the

704   Paris Basin; Correlations of layer proportions, chemical compositions and other data:

705   Bulletin de Minéralogie, v. 106, p. 403-410.

706 Burst, J. F., 1957, Postdiagenetic clay mineral environmental relationships in the Gulf Coast

707   Eocene: Clays & Clay Minerals, v. 6, p. 327-341.

708 -, 1969, Diagenesis of Gulf Coast clayey sediments and its possible relation to petroleum

709   migration: American Association of Petroleum Geologists Bulletin, v. 53, p. 73-93.

710 Chen, Z. S., Tsou, T. C., Asio, V. B., and Tsai, C. C., 2001, Genesis of inceptisols on a

711   volcanic landscape in Taiwan: Soil Science, v. 166, p. 255-266.

712 Claret, F., 2001, Caractérisation structurale des transitions minéralogiques dans les formations

713   argileuses : Contrôles et implications géochimiques des processus d'illitisation. Cas

714   particulier d'une perturbation alcaline dans le Callovo-Oxfordien Laboratoire

715   souterrain Meuse-Haute-Marne, Environnemental and Geochimistry Group: Grenoble,

716   France, Université Joseph Fourrier, p. 174.

717 Claret, F., Sakharov, B. A., Drits, V. A., Velde, B., Meunier, A., Griffault, L., and Lanson, B.,

718   2004, Clay minerals in the Meuse-Haute marne underground laboratory (France):

719   Possible influence of organic matter on clay mineral evolution: Clays and Clay

720   Minerals, v. 52, p. 515-532.

721 Dong, H., 2005, Interstratified illite-smectite: A review of contributions of TEM data to

722   crystal chemical relations and reaction mechanisms: Clay Science, v. 12, Supp. 1, p. 6-

723   12.

724 Dong, H., Peacor, D. R., and Freed, R. L., 1997, Phase relations among smectite, R1 illite-

725   smectite, and illite: American Mineralogist, v. 82, p. 379-391.

726 Douglas, L. A., 1989, Vermiculites, *in* Dixon, J. B., and Weed, S. B., editors, Minerals in Soil

727   Environments: Madison, WI, Soil Science Society of America, p. 635-728.

728 Drits, V. A., and Sakharov, B. A., 1976, X-Ray structure analysis of mixed-layer minerals:

729   Moscow, Nauka, 256 p.

730 Drits, V. A., and Tchoubar, C., 1990, X-ray diffraction by disordered lamellar structures:

731   Theory and applications to microdivided silicates and carbons: Berlin, Springer-

732   Verlag, 371 p.

733   Drits, V. A., Varaxina, T. V., Sakharov, B. A., and Plançon, A., 1994, A simple technique for

734   identification of one-dimensional powder X-ray diffraction patterns for mixed-layer

735   illite-smectites and other interstratified minerals: Clays & Clay Minerals, v. 42, p.

736   382-390.

737   Drits, V. A., Lindgreen, H., Sakharov, B. A., and Salyn, A. L., 1997a, Sequence structure

738   transformation of illite-smectite-vermiculite during diagenesis of Upper Jurassic

739   shales, North Sea: Clay Minerals, v. 32, p. 351-371.

740   Drits, V. A., Srodon, J., and Eberl, D. D., 1997b, XRD measurement of mean crystallite

741   tickness of illite and illite/smectite : Reappraisal of the Kubler index and the Scherrer

742   equation: Clays and Clays Minerals, v. 45, p. 461-475.

743   Drits, V. A., Lindgreen, H., Sakharov, B. A., Jakobsen, H. J., Salyn, A. L., and Dainyak, L.

744   G., 2002a, Tobelitization of smectite during oil generation in oil-source shales.

745   Application to North Sea illite-tobelite-smectite-vermiculite: Clays and Clay Minerals,

746   v. 50, p. 82-98.

747   Drits, V. A., Sakharov, B. A., Dainyak, L. G., Salyn, A. L., and Lindgreen, H., 2002b,

748   Structural and chemical heterogeneity of illite-smectites from Upper Jurassic

749   mudstones of East Greenland related to volcanic and weathered parent rocks:

750   American Mineralogist, v. 87, p. 1590-1606.

751   Drits, V. A., Lindgreen, H., Sakharov, B. A., Jakobsen, H. J., and Zviagina, B. B., 2004, The

752   detailed structure and origin of clay minerals at the cretaceous/tertiary boundary,

753   Stevns Klint (Denmark): Clay Minerals, v. 39, p. 367-390.

754   Drits, V. A., Lindgreen, H., Sakharov, B. A., Jakobsen, H. J., Fallick, A. E., Salyn, A. L.,

755   Dainyak, L. G., Zviagina, B. B., and Barfod, D. N., 2007, Formation and

756   transformation of mixed-layer minerals by tertiary intrusives in cretaceous mudstones,

757   West Greenland: Clays and Clay Minerals, v. 55, p. 260-283.

758   Ferrage, E., Lanson, B., Malikova, N., Plancon, A., Sakharov, B. A., and Drits, V. A., 2005a,

759   New insights on the distribution of interlayer water in bi-hydrated smectite from X-ray

760   diffraction profile modeling of 00l reflections: Chemistry of Materials, v. 17, p. 3499-

761   3512.

762   Ferrage, E., Lanson, B., Sakharov, B. A., and Drits, V. A., 2005b, Investigation of smectite

763   hydration properties by modeling experimental X-ray diffraction patterns: Part I.

764   Montmorillonite hydration properties: American Mineralogist, v. 90, p. 1358-1374.

765   Ferrage, E., Lanson, B., Sakharov, B. A., Geoffroy, N., Jacquot, E., and Drits, V. A., 2007,

766   Investigation of dioctahedral smectite hydration properties by modeling of X-ray

767   diffraction profiles: Influence of layer charge and charge location: American

768   Mineralogist, v. 92, p. 1731-1743.

769   Freed, R. L., and Peacor, D. R., 1992, Diagenesis and the formation of authigenic illite-rich

770   I/S crystals in Gulf Coast shales: TEM study of clay separates: Journal of Sedimentary

771   Petrology, v. 62, p. 220-234.

772   Hoffman, J., and Hower, J., 1979, Clay mineral assemblages as low grade metamorphic

773   geothermometers: Application to the thrust faulted disturbed belt of Montana, U.S.A.,

774   *in* Scholle, P. A., and Schluger, R. P., editors, Aspects of Diagenesis: SEPM Special

775   Publication: Tulsa, Oklahoma, p. 55-79.

776   Howard, S. A., and Preston, K. D., 1989, Profile fitting of powder diffraction patterns, *in*

777   Bish, D. L., and Post, J. E., editors, Modern Powder Diffraction: Reviews in

778   Mineralogy: Wahington D.C., Mineralogical Society of America, p. 217-275.

779   Hower, J., Eslinger, E. V., Hower, M. E., and Perry, E. A., 1976, Mechanism of burial

780   metamorphism of argillaceous sediments: 1. Mineralogical and chemical evidence:

781   Geological Society of America Bulletin, v. 87, p. 725-737.

782   Huang, W. L., 1993, The formation of illitic clays from kaolinite in KOH solution from

783   225°C to 350°C: Clays & Clay Minerals, v. 41, p. 645-654.

784   Inoue, A., and Utada, M., 1983, Further investigations of a conversion series of dioctahedral

785   mica/smectites in the Shinzan hydrothermal alteration area, northeast Japan: Clays &

786   Clay Minerals, v. 31, p. 401-412.

787   Inoue, A., Minato, H., and Utada, M., 1978, Mineralogical properties and occurrence of

788   illite/montmorillonite mixed layer minerals formed from Miocene volcanic glass in

789   Waga-Omono district: Clay Science, v. 5, p. 123-136.

790   Inoue, A., Velde, B., Meunier, A., and Touchard, G., 1988, Mechanism of illite formation

791   during smectite-to-illite conversion in a hydrothermal system: American Mineralogist,

792   v. 73, p. 1325-1334.

793   Inoue, A., Bouchet, A., Velde, B., and Meunier, A., 1989, Convenient technique for

794   estimating smectite layer percentage in randomly interstratified illite/smectite

795   minerals: Clays & Clay Minerals, v. 37, p. 227-234.

796   Inoue, A., Watanabe, T., Kohyama, N., and Brusewitz, A. M., 1990, Characterization of

797   illitization of smectite in bentonite beds at Kinnekulle, Sweden: Clays & Clay

798   Minerals, v. 38, p. 241-249.

799   Inoue, A., Lanson, B., Marques Fernandes, M., Sakharov, B. A., Murakami, T., Meunier, A.,

800   and Beaufort, D., 2005, Illite-smectite mixed-layer minerals in the hydrothermal

801   alteration of volcanic rocks: I. One-dimensional XRD structure analysis and

802   characterization of component layers: Clays and Clay Minerals, v. 53, p. 423-439.

803   Jagodzinski, H., 1949, Eindimensionale Fehlordnung in Kristallen und ihr Einfluss auf die

804   Röntgeninterferenzen: I. Berechnung des Fehlordnungsgrades aus der

805   Röntgenintensitaten: Acta Crystallographica, v. 2, p. 201-207.

806 Jennings, S., and Thompson, G. R., 1986, Diagenesis of Plio-Pleistocene sediments of the

807   Colorado river delta, southern California: Journal of Sedimentary Petrology, v. 56, p.

808   89-98.

809 Kameda, J., Miyawaki, R., Kitagawa, R., and Kogure, T., 2007, XRD and HRTEM analyses

810   of stacking structures in sudoite, di-trioctahedral chlorite: American Mineralogist, v.

811   92, p. 1586-1592.

812 Lanson, B., 2005, Crystal structure of mixed-layer minerals and their X-ray identification:

813   New insights from X-ray diffraction profile modeling: Clay Science, v. 12, Supp. 1, p.

814   1-5.

815 Lanson, B., Sakharov, B. A., Claret, F., and Drits, V. A., 2005, Diagenetic evolution of clay

816   minerals in Gulf Coast shales: New insights from X-ray diffraction profile modeling,

817   42nd Annual Meeting, Clay Minerals Society: Burlington, VT, p. 69.

818 Li, G., Peacor, D. R., and Coombs, D. S., 1997, Transformation of smectite to illite in

819   bentonite and associated sediments from Kaka point, New Zealand: Contrast in rate

820   and mechanism: Clays & Clay Minerals, v. 45, p. 54-67.

821 Lin, C. Y., and Bailey, S. W., 1985, Structural data for sudoite: Clays & Clay Minerals, v. 33,

822   p. 410-414.

823 Lindgreen, H., Drits, V. A., Sakharov, B. A., Salyn, A. L., Wrang, P., and Dainyak, L. G.,

824   2000, Illite-smectite structural changes during metamorphism in black Cambrian

825   Alum shales from the Baltic area: American Mineralogist, v. 85, p. 1223-1238.

826 Lindgreen, H., Drits, V. A., Sakharov, B. A., Jakobsen, H. J., Salyn, A. L., Dainyak, L. G.,

827   and Kroyer, H., 2002, The structure and diagenetic transformation of illite-smectite

828   and chlorite-smectite from North Sea Cretaceous-Tertiary chalk: Clay Minerals, v. 37,

829   p. 429-450.

830   Marques, J. J., Teixeira, W. G., Schulze, D. G., and Curi, N., 2002, Mineralogy of soils with

831   unusually high exchangeable Al from the western Amazon Region: Clay Minerals, v.

832   37, p. 651-661.

833   McCarty, D. K., 2005, XRD pattern simulation of clays and geological interpretation, 42nd

834   Annual Meeting, Clay Minerals Society: Burlington, VT, p. 78.

835   McCarty, D. K., Drits, V. A., Sakharov, B., Zviagina, B. B., Ruffell, A., and Wach, G., 2004,

836   Heterogeneous mixed-layer clays from the Cretaceous greensand, Isle of Wight,

837   southern England: Clays and Clay Minerals, v. 52, p. 552-575.

838   McCarty, D. K., Drits, V. A., and Sakharov, B. A., 2005, Advantages and limitations of

839   simulation of XRD patterns of clays: Mod-1 to present, 42nd Annual Meeting, Clay

840   Minerals Society: Burlington, VT, p. 76.

841   McCarty, D. K., Sakharov, B. A., and Drits, V. A., 2008, Early clay diagenesis in Gulf Coast

842   sediments: New insights from XRD profile modeling: Clays & Clay Minerals, p. in

843   press.

844   Méring, J., 1949, L'interférence des rayons-X dans les systèmes à stratification désordonnée:

845   Acta Crystallographica, v. 2, p. 371-377.

846   Moore, D. M., and Reynolds, R. C., Jr, 1997, X-ray Diffraction and the Identification and

847   Analysis of Clay Minerals, Oxford University Press, 378 p.

848   Nadeau, P. H., and Reynolds, R. C., Jr, 1981, Burial and contact metamorphism in the

849   Mancos Shale: Clays & Clay Minerals, v. 29, p. 249-259.

850   Perry, E. A., Jr, and Hower, J., 1970, Burial diagenesis in Gulf Coast pelitic sediments: Clays

851   & Clay Minerals, v. 18, p. 165-177.

852   -, 1972, Late-stage dehydration in deeply buried pelitic sediments: American Association of

853   Petroleum Geologists Bulletin, v. 56, p. 2013-2021.

854 Pytte, A. M., and Reynolds, R. C., 1989, The thermal transformation f smectite to illite, *in*

855   Naeser, N. D., and McCulloh, T. H., editors, Thermal history of sedimentary basins:

856   New York, Springer, p. 133-140.

857 Reynolds, R. C., Jr, 1967, Interstratified clay systems: Calculation of the total one-

858   dimensional diffraction function: American Mineralogist, v. 52, p. 661-672.

859 -, 1980, Interstratified clay minerals, *in* Brindley, G. W., and Brown, G., editors, Crystal

860   structures of clay minerals and their X-ray identification: London, The Mineralogical

861   Society, p. 249-359.

862 -, 1986, The Lorentz-polarization factor and preferred orientation in oriented clay aggregates:

863   Clays & Clay Minerals, v. 34, p. 359-367.

864 Reynolds, R. C., Jr, and Hower, J., 1970, The nature of interlayering in mixed-layer illite-

865   montmorillonites: Clays & Clay Minerals, v. 18, p. 25-36.

866 Sakharov, B. A., and Drits, V. A., 1973, Mixed-layer kaolinite-montmorillonite: A

867   comparison of observed and calculated diffraction patterns: Clays & Clay Minerals, v.

868   21, p. 15-17.

869 Sakharov, B. A., Lindgreen, H., and Drits, V. A., 1999a, Mixed-layer kaolinite-illite-

870   vermiculite in North Sea shales: Clay Minerals, v. 34, p. 333-344.

871 Sakharov, B. A., Lindgreen, H., Salyn, A., and Drits, V., 1999b, Determination of illite-

872   smectite structures using multispecimen XRD profile fitting.: Clays and Clays

873   Minerals, v. 47, p. 555-566.

874 Sakharov, B. A., Dubinska, E., Bylina, P., Kozubowski, J. A., Kapron, G., and Frontczak

875   Baniewicz, M., 2004, Serpentine-smectite interstratified minerals from Lower Silesia

876   (SW Poland): Clays and Clay Minerals, v. 52, p. 55-65.

877 Shutov, V. D., Drits, V. A., and Sakharov, B. A., 1969, On the mechanism of a

878   postsedimentary transformation of montmorillonite into hydromica, *in* Heller, L.,

879   editor, International Clay Conference: Tokyo, Japan, Israel University Press,

880   Jerusalem, p. 523-531.

881 Srodon, J., 1978, Correlation between coal and clay diagenesis in the Carboniferous of the

882   upper Silesian coal basin, *in* Mortland, M. M., and Farmer, V. C., editors,

883   International Clay Conference: Oxford, Elsevier, p. 251-260.

884 -, 1980, Precise identification of illite/smectite interstratifications by X-ray powder

885   diffraction: Clays & Clay Minerals, v. 28, p. 401-411.

886 -, 1981, X-Ray identification of randomly interstratified illite-smectite in mixtures with

887   discrete illite: Clay Minerals, v. 16, p. 297-304.

888 -, 1984a, Mixed-layer illite-smectite in low-temperature diagenesis: Data from the Miocene of

889   the Carpathian foredeep: Clay Minerals, v. 19, p. 205-215.

890 -, 1984b, X-ray powder diffraction of illitic materials: Clays & Clay Minerals, v. 32, p. 337-

891   349.

892 -, 1999, Nature of mixed-layer clays and mechanisms of their formation and alteration:

893   Annual Review of Earth and Planetary Sciences, v. 27, p. 19-53.

894 Srodon, J., and Eberl, D. D., 1984, Illite, *in* Bailey, S. W., editor, Micas: Reviews in

895   Mineralogy: Washington DC, Mineralogical Society of America, p. 495-544.

896 Srodon, J., Eberl, D. D., and Drits, V. A., 2000, Evolution of fundamental-particle size during

897   illitization of smectite and implications for reaction mechanism: Clays and Clay

898   Minerals, v. 48, p. 446-458.

899 Sucha, V., Kraus, I., Gerthofferova, H., Petes, J., and Serekova, M., 1993, Smectite to illite

900   conversion in bentonites and shales of the East Slovak basin: Clay Minerals, v. 28, p.

901   243-253.

902 Sudo, T., and Shimoda, S., 1977, Interstratified clay minerals - Mode of occurrence and

903   origin: Minerals Sci. Engng., v. 9, p. 3-24.

904   Velde, B., and Brusewitz, A. M., 1982, Metasomatic and non-metasomatic low grade
905   metamorphism of Ordovician meta-bentonites in Sweden: Geochimica &
906   Cosmochimica Acta, v. 46, p. 447-452.

907   -, 1986, Compositional variation in component layers in natural illite/smectite: Clays & Clay
908   Minerals, v. 34, p. 651-657.

909   Velde, B., and Iijima, A., 1988, Comparison of clay and zeolite mineral occurrences in
910   Neogene age sediments from several deep wells: Clays & Clay Minerals, v. 36, p.
911   337-342.

912   Velde, B., and Espitalié, J., 1989, Comparison of kerogen maturation and illite/smectite
913   composition in diagenesis: Journal of Petroleum Geology, v. 12, p. 103-110.

914   Velde, B., and Vasseur, G., 1992, Estimation of the diagenetic smectite to illite transformation
915   in time-temperature space: American Mineralogist, v. 77, p. 967-976.

916   Velde, B., Suzuki, T., and Nicot, E., 1986, Pressure-Temperature-Composition of
917   illite/smectite mixed-layer minerals: Niger delta mudstones and other examples: Clays
918   & Clay Minerals, v. 34, p. 435-441.

919   Watanabe, T., 1981, Identification of illite/montmorillonite interstratification by X-ray
920   powder diffraction: Journal of the Mineralogical Society of Japan, v. Spec. Issue 15, p.
921   32-41.

922   -, 1988, The structural model of illite/smectite interstratified mineral and the diagram for their
923   identification: Clay Science, v. 7, p. 97-114.

924   Weaver, C. E., 1957, The clay petrology of sediments: Clays and Clay Minerals, v. 6, p. 154-
925   187.

926   -, 1959, Possible uses of clay minerals in search for oil: Clays and Clay Minerals, v. 8, p. 214-
927   227.

928   Whitney, G., 1990, Role of water in the smectite-to-illite reaction: Clays & Clay Minerals, v.

929   38, p. 343-350.

930   Whitney, G., and Northrop, H. R., 1988, Experimental investigation of the smectite to illite

931   reaction: Dual reaction mechanisms and oxygen-isotope systematics: American

932   Mineralogist, v. 73, p. 77-90.

933

934

935   Fig. 1. Age of the sediments as a function of depth in Carter and Mustang Island wells

936   (top − Velde and Vasseur, 1992). Smectite content in I-Exp as determined by Velde and

937   Vasseur (1992) as a function of depth in these two wells.

938   Fig. 2. Experimental XRD patterns obtained from Carter well samples selected as being

939   representative of the complete smectite-to-illite diagenetic transition. Sampling depths are

940   2170 (A), 3660 (B), 4000 (C), 4640 (D), 5010 (E), and 5180 m (F). XRD patterns obtained on

941   EG solvated samples. Dashed and dot-dashed lines indicate the positions of illite and smectite

942   reflections. Solid and dot-dot-dashed lines indicate positions of some kaolinite and chlorite

943   reflections. For all samples, the gray bar indicates a modified scale factor for the high-angle

944   region.

945   Fig. 3. Comparison between experimental XRD patterns obtained from Carter well

946   samples investigated in the present study and those obtained by Perry and Hower (1970) on

947   selected samples from well E (Galveston county). The latter samples were used to establish

948   the smectite-to-illite diagenetic transition in Gulf Coast clay-rich sediments. XRD patterns

949   obtained on EG solvated samples.

950   Fig. 4. Comparison between experimental and calculated XRD patterns as a function of

951   depth for group I samples (single-phase segregated I-Exp model). Experimental and

952   calculated optimal XRD patterns are shown as crosses and as solid lines, respectively.

953   Optimal structure models are described in tables 1 and 2. For all samples, the gray bar

954   indicates a modified scale factor for the high-angle region. **A**. XRD patterns obtained on EG

955   solvated samples. **B**. XRD patterns obtained on air-dried samples at 40% relative humidity.

956   Fig. 5. Comparison between experimental and calculated XRD patterns as a function of

957   depth for all Carter well samples (mixture model). Experimental and calculated optimal XRD

958 patterns are shown as crosses and as solid lines, respectively. Optimal structure models are

959 described in tables 4 and 5. For all samples, the gray bar indicates a modified scale factor for

960 the high-angle region. **A**. XRD patterns obtained on EG solvated samples. **B**. XRD patterns

961 obtained on air-dried samples at 40% relative humidity.

962   Fig. 6. Sensitivity of calculated XRD patterns to the mineralogical composition.

963 Patterns as for figure 5. Arrows indicate significant misfit as compared to the optimum fits

964 shown in figure 5. The optimum mineralogical composition is given in table 5. **A**. Sample B –

965 3660 m Ca-saturated after EG solvation without the contribution of discrete smectite. **B**.

966 Sample B – 3660 m Ca-saturated after EG solvation without the contribution of K-Exp.

967   Fig. 7. Sensitivity of calculated XRD patterns to the mineralogical composition.

968 Patterns as for figure 5. Arrows indicate significant misfit as compared to the optimum fits

969 shown in figure 5. The optimum mineralogical composition is given in table 5. **A**. Sample E –

970 5010 m Ca-saturated after EG solvation without the contribution of I-Exp. **B**. Sample E –

971 5010 m Ca-saturated air-dried without the contribution of I-Exp. **C**. Sample E – 5010 m Ca-

972 saturated air-dried without the contribution of I-Exp-Ch.

973   Fig. 8. Sensitivity of calculated XRD patterns to structural parameters. Patterns as for

974 figure 5. Arrows indicate significant misfit as compared to the optimum fits shown in figure

975 5. The structural parameters for the optimal models are given in table 4. **A**. Sample E –

976 5010 m Ca-saturated air-dried. In I-Exp-Ch, Ch layers (with 3.0 Mg and 6.0 OH per half unit-

977 cell in their interlayers) are replaced by Exp layers (with 0.25 Mg and 2.0 OH per half unit-

978 cell in their interlayers). **B**. Sample B – 3660 m Ca-saturated air-dried. In I-Exp, 14.0 Å Exp

979 layers (8% of the layers) are replaced by 15.0 Å Exp layers. **C**. Sample B – 3660 m Ca-

980 saturated air-dried. In I-Exp, 14.0 Å Exp layers (8% of the layers) are replaced by 12.5 Å Exp

981 layers.

982

Table 1A. Single-phase segregated I-Exp model. Composition and structural parameters of the segregated I-Exp in group I samples.

Sample	W_I	W_{Exp1}	W_{Exp2}	W_{Exp3}	h_{Exp1}	h_{Exp2}	h_{Exp3}	R	N_{av}	N_{max}	S_q
A – EG	0.45	0.55	-	-	16.76	-	-	1	7	50	
A – AD	0.45	0.30	0.15	0.10	15.00	12.50	14.00	1	7	50	0.27
B – EG	0.65	0.27	0.08	-	16.76	14.00	-	1	15	50	
B – AD	0.65	0.21	0.14	-	15.00	12.50	-	1	15	50	0.19
C – EG	0.65	0.27	0.08	-	16.76	14.00	-	1	15	50	
C – AD	0.65	0.15	0.20	-	14.90	12.50	-	1	15	50	0.10

Note: The basal d_{001} distances of the different layer types (h_i) are given in Å. R is the Reichweit parameter (Jagodzinski, 1949) which characterizes the extent of ordering as the number of adjacent layers influencing the nature of a given layer. N_{av} and N_{max} are the average and maximum numbers of layers in coherent scattering domains (lognormal size distribution). S_q parameter is an estimator of the degree of segregation in I-Exp (eq 1).

Table 1B. Single-phase segregated I-Exp model. Junction probabilities of the segregated I-Exp in samples A, B, and C.

A-AD	I 9.98 Å	Exp1 15.00 Å	Exp2 12.50 Å	Exp3 14.00 Å
I (9.98 Å) 0.45	0.600	0.133	0.133	0.133
Exp1 (15.00 Å) 0.30	0.200	0.500	0.167	0.133
Exp2 (12.50 Å) 0.15	0.400	0.333	0.267	0.000
Exp3 (14.00 Å) 0.10	0.600	0.400	0.000	0.000

A-EG	I 9.98 Å	Exp 16.76 Å
I (9.98 Å) 0.45	0.600	0.400
Exp (16.76 Å) 0.55	0.327	0.673

B-AD	I 9.98 Å	Exp1 15.00 Å	Exp2 12.50 Å
I (9.98 Å) 0.65	0.716	0.178	0.106
Exp1 (15.00 Å) 0.21	0.520	0.350	0.130
Exp2 (12.50 Å) 0.14	0.537	0.150	0.313

B-EG	I 9.98 Å	Exp1 16.76 Å	Exp2 14.00 Å
I (9.98 Å) 0.65	0.716	0.216	0.068
Exp1 (16.76 Å) 0.27	0.520	0.480	0
Exp2 (14.00 Å) 0.08	0.550	0	0.450

C-AD	I 9.98 Å	Exp1 15.00 Å	Exp2 12.50 Å
I (9.98 Å) 0.65	0.684	0.138	0.178
Exp1 (14.90 Å) 0.15	0.600	0.150	0.250
Exp2 (12.50 Å) 0.20	0.580	0.240	0.180

C-EG	I 9.98 Å	Exp1 16.76 Å	Exp2 14.00 Å
I (9.98 Å) 0.65	0.683	0.249	0.068
Exp1 (16.76 Å) 0.27	0.600	0.400	0
Exp2 (14.00 Å) 0.08	0.550	0	0.450

Table 2. Single-phase segregated I-Exp model. Relative proportions (in wt%) of the different contributions to the diffracted intensity.

Sample	I-Exp	Ill	Kaol	Ch	K-Exp[a]	R_{wp}[b]	R_{exp}[b]
A – EG	79	5	11	-	5	11.42%	1.73%
A – AD	79	5	11	-	5	11.00%	1.64%
B – EG	64	10	9	1	16	11.60%	2.36%
B – AD	57	13	9	2	19	10.80%	2.05%
C – EG	55	18	8	1	18	11.31%	1.94%
C – AD	52	25	8	2	13	9.85%	1.85%

[a] The composition of K-Exp is constant (75:25 K:Exp ratio).
[b] Estimators of the fit quality (R_{wp}) and of the statistical error associated with measured intensities (R_{exp} – Howard and Preston, 1989)).

Table 3. Single-phase segregated I-Exp model. Relative abundance of the different layers and layer pairs (W_i and W_{ij} parameters) for the segregated I-Exp in group I samples.

Layer sequence	A sample	B sample	C sample
I	0.45	0.65	0.65
Exp	0.55	0.35	0.35
II	0.270	0.465	0.444
IExp	0.180	0.184	0.206
ExpI	0.180	0.184	0.206
ExpExp	0.370	0.166	0.144

Table 4A. Mixture model. Composition and structural parameters of I-Exp in group I samples.

Sample	Phase	W_I	W_{Exp1}	W_{Exp2}	W_{Exp3}	h_{Exp1}	h_{Exp2}	h_{Exp3}	N_{av}	N_{max}	R	Junction probability parameters
A – EG	I-Exp	0.57	0.35	0.08	-	16.70	14.00	-	12	50	0	$R = 0$ ($P_{ij} = W_j$)
A – AD	I-Exp	0.57	0.20	0.08	0.15	15.00	14.00	12.50	12	50	0	-
B – EG	I-Exp	0.62	0.30	0.08	-	16.72	14.00	-	12	50	0	-
B – AD	I-Exp	0.62	0.15	0.08	0.15	15.00	14.00	12.50	12	50	0	-
C – EG	I-Exp	0.67	0.30	0.03	-	16.85	14.00	-	12	50	0	-
C – AD	I-Exp	0.67	0.17	0.03	0.13	15.00	14.00	12.50	12	50	0	-

The basal d_{001} distances of the different layer types (h_i) are given in Å. R is the Reichweit parameter (Jagodzinski, 1949) which characterizes the extent of ordering as the number of adjacent layers influencing the nature of a given layer. N_{av} and N_{max} are the average and maximum numbers of layers in coherent scattering domains (lognormal size distribution).

Table 4B. Mixture model. Composition and structural parameters of K-Exp.

Sample	Phase	W_I	W_{Exp1}	W_{Exp2}	H_K	h_{Exp1}	h_{Exp2}	N_{av}	N_{max}	R	Junction probability parameters
A – EG	K-Exp	0.75	0.10	0.15	7.156	16.90	12.90	12	50	0	$R = 0$ ($P_{ij} = W_j$)
A – AD	K-Exp	0.75	0.05	0.20	7.156	15.00	12.50	12	50	0	-
B – EG	K-Exp	0.75	0.00	0.25	7.156	16.90	12.90	12	50	0	-
B – AD	K-Exp	0.75	0.00	0.25	7.156	15.00	12.50	12	50	0	-
C – EG	K-Exp	0.75	0.10	0.15	7.156	16.90	12.90	12	50	0	-
C – AD	K-Exp	0.75	0.00	0.25	7.156	15.00	12.50	12	50	0	-
D – EG	K-Exp	0.75	0.15	0.10	7.156	16.90	12.90	12	50	0	-
D – AD	K-Exp	0.75	0.05	0.20	7.156	15.00	12.50	12	50	0	-
E – EG	K-Exp	0.75	0.15	0.10	7.156	16.90	12.90	12	50	0	-
E – AD	K-Exp	0.75	0.00	0.25	7.156	15.00	12.50	12	50	0	-
F – EG	K-Exp	0.75	0.10	0.15	7.156	16.90	12.90	12	50	0	-

The basal d_{001} distances of the different layer types (h_i) are given in Å. R is the Reichweit parameter (Jagodzinski, 1949) which characterizes the extent of ordering as the number of adjacent layers influencing the nature of a given layer. N_{av} and N_{max} are the average and maximum numbers of layers in coherent scattering domains (lognormal size distribution).

Table 4C. Mixture model. Composition and structural parameters of the mixed layers in group II samples.

Sample	Phase	W_I	W_{Exp1}	W_{Exp2}	W_{Ch}	h_{Exp1}	h_{Exp2}	h_{Ch}	N_{av}	N_{max}	R	Junction probability parameters
D – EG	I-Exp	0.70	0.25	0.05		16.86	12.90		15	100	1	R = 1 with MPDO[a] $P_{Exp1Exp1} = P_{Exp1Exp2} = 0$ $P_{Exp2Exp1} = P_{Exp2Exp2} = 0$
	I-Exp-Ch	0.70	0.15	-	0.15	16.86		14.00[b]	12	50	1	$P_{Exp1Exp1} = P_{Exp1Ch} = P_{ChExp1} = 0.150$ $P_{ChCh} = 0.265$
D – AD	I-Exp	0.70	0.30			15.00			15	100	1	R = 1 with MPDO[a] $P_{Exp1Exp1} = 0$
	I-Exp-Ch	0.70	0.05	0.10	0.15	15.00	12.50	14.00[b]	12	50	1	$P_{Exp1Exp1} = P_{Exp2Exp1} = P_{ChExp1} = 0.050$ $P_{Exp1Exp2} = P_{Exp2Exp2} = P_{ChExp2} = 0.100$ $P_{Exp1Ch} = P_{Exp2Ch} = 0.150$ $P_{ChCh} = 0.265$
E – EG	I-Exp	0.75	0.21	0.04		16.92	12.90		15	100	2	$P_{Exp1Exp1} = P_{Exp1Exp2} = P_{Exp2Exp1} = P_{Exp2Exp2} = 0$ $P_{Exp1IExp1} = 0.350^b$
	I-Exp-Ch	0.70	0.15		0.15	16.86		14.00[b]	12	50	1	$P_{Exp1Exp1} = P_{Exp1Ch} = P_{ChExp1} = 0.150$ $P_{ChCh} = 0.265$
E – AD	I-Exp	0.75	0.21	0.04		15.00	12.50		15	100	2	$P_{Exp1Exp1} = P_{Exp1Exp2} = P_{Exp2Exp1} = P_{Exp2Exp2} = 0$ $P_{Exp1IExp1} = 0.350^b$
	I-Exp-Ch	0.70		0.15	0.15		12.50	14.00[b]	12	50	1	$P_{Exp1Exp1} = P_{Exp1Ch} = P_{ChExp1} = 0.150$ $P_{ChCh} = 0.265$
F – EG	I-Exp	0.75	0.20	0.05		16.86	12.90		15	100	2	$P_{Exp1Exp1} = P_{Exp1Exp2} = P_{Exp2Exp1} = P_{Exp2Exp2} = 0$

									$P_{Exp1|Exp1} = 0.300$, $P_{Exp1|Exp2} = 0.050^{c}$
I-Exp-Ch	0.70	0.10	0.20	16.86	14.00[b]	12	50	1	$P_{Exp1Exp1} = P_{Exp1Ch} = P_{ChExp1} = 0.150$
									$P_{ChCh} = 0.265$

[a] Maximum possible degree of ordering which prohibits pairs of the minor layers: $P_{jj} = 0$ if $W_j < 0.5$. Refer to Reynolds (1980), Drits and Tchoubar (1990), and Moore and Reynolds (1997) for additional details.

[b] Other junction probability parameters needed to describe layer stacking are $P_{Exp1|Exp2} = P_{Exp2|Exp1} = P_{Exp2|Exp2} = 0$

[c] Other junction probability parameters needed to describe layer stacking are $P_{Exp2|Exp1} = P_{Exp2|Exp2} = 0$

Table 5. Mixture model. Relative proportions (in wt%) of the different contributions to the diffracted intensity.

Sample	I-Exp	I-Exp-Ch	Sm	Ill	Kaol	Ch	K-Exp	R_{wp}[a]	R_{exp}[a]
A – EG	45	-	27	4	9	-	15	9.14%	1.73%
A – AD	43	-	26	6	11	-	14	8.06%	1.64%
B – EG	51	-	5	15	14	2	13	14.16%	2.36%
B – AD	50	-	5	19	12	2	12	9.30%	2.05%
C – EG	57	-	2	21	6	2	12	11.12%	1.94%
C – AD	58	-	3	22	7	2	8	9.72%	1.85%
D – EG	42	26	-	10	6	4	12	8.23%	2.28%
D – AD	39	28	-	9	5	4	15	8.99%	1.15%
E – EG	34	30	-	9	11	4	12	10.23%	2.11%
E – AD	31	32	-	6	12	5	14	11.94%	2.00%
F – EG	34	42	-	5	7	5	7	13.38%	3.07%

[a] Estimators of the fit quality (R_{wp}) and of the statistical error associated with measured intensities (R_{exp} – Howard and Preston, 1989).

Table 6. Mixture model. Relative abundance of the different layers and layer pairs (W_i and W_{ij} parameters) in the I-Exp of samples C and D.

Layer sequence	C sample	D sample
I	0.670	0.700
Exp1	0.300	0.250
Exp2	0.030	0.050
II	0.449	0.400
IExp1	0.201	0.250
IExp2	0.020	0.050
Exp1I	0.201	0.250
Exp1Exp1	0.090	0.000
Exp1Exp2	0.009	0.000
Exp2I	0.020	0.050
Exp2Exp1	0.009	0.000
Exp2Exp2	0.001	0.000

Table 7. Mixture model. Junction probabilities of mixed layers occurring during the hypothesized solid-state transformation of I-Exp from sample C to I-Exp-Ch from sample D. The composition and structural parameters (segregation of I and Exp layers) of these mixed layers are thus theoretically intermediate between those of the two end members.

Layer sequence	Sample C	Inter. Phase I	Inter. phase II	Sample D
W_I	0.670	0.680	0.690	0.700
W_{Exp}	0.330	0.270	0.210	0.150
W_{Ch}	0.000	0.050	0.100	0.150
S_q - I	0.000	0.027	0.054	0.083
S_q - Ch	0.000	0.045	0.090	0.135
P_{II}	0.670	0.689	0.707	0.725
P_{IExp}	0.330	0.264	0.205	0.150
P_{ICh}	0.000	0.047	0.088	0.125
P_{ExpI}	0.670	0.680	0.690	0.700
P_{ExpExp}	0.330	0.270	0.210	0.150
P_{ExpCh}	0.000	0.050	0.100	0.150
P_{ChI}	-	0.561	0.573	0.585
P_{ChExp}	-	0.346	0.246	0.150
P_{ChCh}	-	0.093	0.181	0.265

Note: S_q is an estimator of the degree of segregation of I and Ch layers in I-Exp-Ch (eq 1).

APPENDIX

882

883 *Single-phase segregated I-Exp model: Self-consistency of the model*.

884 For a given sample, junction probability parameters, P_{ij}, refined for the I-Exp

885 contribution are different for AD and EG states (table 1B). This apparent inconsistency arises

886 from the contrasting expansion behavior of Exp layers in AD and EG states. For example, the

887 hydration behavior of Exp layers is highly heterogeneous in sample A with three types of Exp

888 layers, whereas EG solvation results in the homogeneous swelling of all Exp layers to

889 16.76 Å (2EG). However, the distribution of illite and expandable layers in I-Exp should be

890 identical in both states. Therefore, the four-component I-Exp in sample A (AD state) must be

891 reduced to a two-component system following EG solvation if the 15.0, 14.0 and 12.5 Å

892 layers become 2EG layers. To ensure the consistency of the structure model for sample A the

893 sums $(W_{Exp1I} + W_{Exp2I} + W_{Exp3I})$, $(W_{IExp1} + W_{IExp2} + W_{IExp3})$, and $(W_{Exp1Exp1} + W_{Exp1Exp2} +$

894 $W_{Exp1Exp3} + W_{Exp2Exp1} + W_{Exp2Exp2} + W_{Exp2Exp3} + W_{Exp3Exp1} + W_{Exp3Exp2} + W_{Exp3Exp3})$ obtained

895 for the four-component I-Exp (AD state) must be equal to the parameters W_{ExpI}, W_{IExp} and

896 W_{ExpExp}, respectively, determined for the two-component I-Exp following EG solvation (table

897 1B). Here, $W_{ij} = W_i P_{ij}$ is the occurrence probability for an ij layer pair (i, j = I, Exp, Exp_1,

898 Exp_2 and Exp_3 – Exp, Exp_1, Exp_2 and Exp_3 denote 16.76, 15.0, 12.5 and 14.0 Å layers). W_{ij}

899 parameters are reported in table A-1 for I-Exp in group I samples. For sample A, $W_{II} = 0.270$

900 in both AD and EG states and the above relationships are valid. In samples B and C, two

901 types of expandable layers coexist in both AD and EG states. However, the relative amounts

902 of the two types differ in AD and EG states, thus leading to contrasting values of P_{ij}

903 parameters for the corresponding models (table 1B). To ensure the consistency of the

904 proposed models these parameters can be reconciled by considering that some of the

905　　expandable layers (noted as Exp' layers in tables A-1B, C) behave as Exp2 layers in the AD

906　　state and as Exp1 layers when EG solvated (tables A-1B, C).

907

908　　*Possible solid-state formation of I-Exp-Ch (sample D) at the expense of I-Exp (sample C)*

909　　　　　As described in the main text, the contents of illite layers in I-Exp from sample C and in

910　　I-Exp-Ch from sample D are similar (67 and 70%I, respectively). Junction probability

911　　parameters exhibit also strong similarities, interstratification being random in I-Exp from

912　　sample C, and showing only slight tendency to segregation in I-Exp-Ch from sample D (table

913　　4). In addition, I-Exp from sample C and I-Exp-Ch from sample D have similar CSD sizes.

914　　As a consequence, a solid-state mechanism can be hypothesized for the transition between the

915　　two mixed layers, and a series of mixed layers with compositions and structural features (for

916　　example the segregation degree of I and Ch Layers, and the random interstratification of Exp

917　　layers) intermediate between those of the two end members can be envisaged (table 7). The

918　　scope of this section is to describe in detail this hypothesized solid-state transformation and to

919　　assess its robustness from the analysis of the relative abundance of layer pairs and triplets

920　　(W_{ij}, and W_{ijk}, respectively – i, j, k = I, Exp, Ch) and of their evolution during the

921　　transformation. This evolution should follow logically from that of the relative proportion of

922　　the different layer types and of their layer stacking.

923　　　　　For this purpose, relative abundances of layer pairs and triplets deduced from structure

924　　models (W_{XRD} in table A-2) serve as the basis for this analysis. The first step is thus to

925　　calculate the occurrence probabilities for layer pairs and triplets in I-Exp from sample C, in I-

926　　Exp-Ch from sample D, and in the two intermediate phases. These occurrence probabilities

927　　can be calculated from the junction probabilities listed in table 7 ($W_{ij} = W_i P_{ij}$, and $W_{ijk} =$

928　　$W_{ij} P_{jk}$) and are reported in table A-2 (columns W_{XRD}). The second step is to identify layer

929　　pairs whose occurrence probability deduced from structure models (columns W_{XRD}) is

930   decreasing along the reaction pathway (from I-Exp in sample C to phase I to phase II and

931   finally to I-Exp-Ch in sample D). For example, from I-Exp in sample C to phase I, the

932   occurrence probabilities of IExp, ExpI and ExpExp pairs (W_{IExp}, W_{ExpI}, W_{ExpExp}) are

933   decreasing. In table A-2 such pairs are identified with an arrow following their occurrence

934   probability. The third step is to distribute these layer pairs so as to match the occurrence

935   probabilities of layer pairs in the next phase (phase I in our example) as shown in table A-3A.

936   In our example, 0.1798 out of the initial 0.2211 IExp pairs are preserved whereas 0.0319 pairs

937   are transformed to ICh pair, as required for intermediate phase I, the remaining 0.0094 pairs

938   being transformed to II pairs. The same procedure can be applied to ExpI and ExpExp pairs.

939   As a result, theoretical occurrence probabilities can be calculated for all layer pairs in phase I,

940   phase II, and in the I-Exp-Ch from sample D. These values are reported in the W_{Cal} columns

941   of table A-2, and they systematically coincide with W_{XRD} values. The fourth step is to

942   calculate occurrence probabilities for all layer triplets. Again, this starts with the identification

943   of the layer triplets whose occurrence probability deduced from structure models (columns

944   W_{XRD}) is decreasing along the reaction pathway (from I-Exp in sample C to phase I to phase

945   II and finally to I-Exp-Ch in sample D). For example, from I-Exp in sample C to phase I, the

946   occurrence probabilities of IIExp, IExpI, IExpExp, ExpII, ExpIExp, ExpExpI, and

947   ExpExpExp triplets (W_{IIExp}, W_{IExpI}, $W_{IExpExp}$, W_{ExpII}, $W_{ExpIExp}$, $W_{ExpExpI}$, and $W_{ExpExpExp}$) are

948   decreasing. In table A-2 such triplets are identified with an arrow following their occurrence

949   probability. To distribute these "disappearing" layer triplets among newly formed ones, the

950   R = 1 Reichweit parameter implies that the transition probability from one layer pair to

951   another does not depend on the preceding or following layer. As an illustration, one may

952   consider the transformation of the 0.1481 IIExp triplets present in I-Exp from sample C. As

953   IExp pairs may be transformed to II, IExp, and ICh pairs (table A-3A) IIExp triplets are

954   transformed to III, IIExp, and IICh triplets (0.0063 = 0.1481 × 0.0094 ÷ 0.2211, 0.1204 =

955 0.1481 × 0.1798 ÷ 0.2211, and 0.0214 = 0.1481 × 0.0319 ÷ 0.2211, respectively). In this case,

956 the initial layer pair (II) is not modified during transformation from I-Exp in sample C to

957 intermediate phase I. If both the initial and final layer pairs of a triplet are modified (such as

958 for IExpI triplets from sample C), the two modifications have to be considered separately.

959 Transformation of the first layer pair (IExp) leads to the formation of III, IExpI, and IChI

960 triplets, whereas that of the second layer pair (ExpI) leads to III, IExpI, and IExpCh triplets.

961 Relative proportions of the newly formed layer triplets are calculated as described above

962 (0.0031 = 0.1481 × 0.0094 ÷ (0.2211 + 0.2211), 0.0602 = 0.1481 × 0.1798 ÷ (0.2211 +

963 0.2211), 0.0214 = 0.1481 × 0.0319 ÷ (0.2211 + 0.2211), 0.0032 = 0.1481 × 0.0095 ÷

964 (0.2211 + 0.2211), et cetera). These values are reported in table A-3B for all layer triplets and

965 for the different transitions. They can be summed up to calculate theoretical occurrence

966 probabilities for all layer triplets in phase I, phase II, and in the I-Exp-Ch from sample D that

967 are reported in the W_{Cal} columns of table A-2. These values are very similar to those

968 calculated from the XRD structure models determined for I-Exp from sample C and for I-

969 Exp-Ch from sample D, and hypothesized for intermediate phases I and II. Following the

970 transition from I-Exp (sample C) to phase I, differences between W_{Cal} and W_{XRD} are

971 maximum for ExpIExp (0.0115), ChExpI (-0.0080), IExpExp (0.0074), and ExpExpI (0.0069)

972 triplets. For the phase I to phase II transition, these differences are most substantial for

973 ExpIExp (0.0085) and ExpExpI (0.0061) triplets. For the transition from phase II to I-Exp-Ch

974 (sample D), only IChCh and ChChI layer triplets present non-negligible differences between

975 the W_{Cal} and W_{XRD} (-0.0079, and -0.0065, respectively). Overall, the observed agreement

976 between calculated W_{ijk} values and those derived from structure models is excellent and

977 supports the hypothesized solid-state reaction mechanism as it is strongly influenced by the

978 choice of junction probability parameters. In particular, if the $P_{SS} = W_S$ is not maintained for

979 intermediate phases, calculated W_{ijk} values differ significantly from those derived from

980   structure models. However, I-Exp-Ch structure models hypothesized for intermediate phases I

981   and II and layer pair transitions are to be considered only as an approximation to the actual

982   mechanism of I-Exp-Ch formation at the expense of I-Exp.

Fig. A-1. Experimental XRD patterns obtained from Carter well samples selected as being representative of the complete smectite-to-illite diagenetic transition. Sampling depths are 2170 (A), 3660 (B), 4000 (C), 4640 (D), 5010 (E), and 5180 m (F). Data collected on air-dried samples at 40% relative humidity. Patterns as in figure 1.

Fig. A-2. Elementary contributions to the intensity diffracted by sample B (3660 m). Patterns as for figure 5. The structural parameters for the optimal models are given in table 4A. **A**. Air-dried sample. **B**. EG solvated sample.

Fig. A-3. Elementary contributions to the intensity diffracted by sample E (5010 m). Patterns as for figure 5. The structural parameters for the optimal models are given in table 4C. **A**. Air-dried sample. **B**. EG solvated sample.

Fig. A-4. Sensitivity of calculated XRD patterns to structural parameters. Patterns as for figure 5. **A**. Sample E – 5010 m Ca-saturated air-dried. Elementary contribution of the optimum I-Exp-Ch (table 4C). **B**. Sample E – 5010 m Ca-saturated air-dried. 14.0 Å Ch layers (with 3.0 Mg and 6.0 OH per half unit-cell in their interlayers) of the optimum I-Exp-Ch are replaced by 14.0 Å Exp layers (with 0.25 Mg and 2.0 OH per half unit-cell in their interlayers).

Table A-1A. Single-phase segregated I-Exp model. Relative abundance of the different layer pairs (W_{ij} parameters) calculated for the segregated I-Exp from sample A.

A-AD	I 9.98 Å	Exp1 15.00 Å	Exp2 12.50 Å	Exp3 14.00 Å
I 9.98 Å	0.270	0.060	0.060	0.060
Exp1 15.00 Å	0.060	0.150	0.050	0.040
Exp2 12.50 Å	0.060	0.050	0.040	0.000
Exp3 14.00 Å	0.060	0.040	0.000	0.000

A-EG	I 9.98 Å	Exp 16.76 Å
I 9.98 Å	0.270	0.180
Exp 16.76 Å	0.180	0.370

Note: The W_{ij} matrices obtained for AD and EG states are equivalent if Exp_{EG} = $Exp1_{AD}$ + $Exp2_{AD}$ + $Exp3_{AD}$.

Table A-1B. Single-phase segregated I-Exp model. Relative abundance of the different layer pairs (W_{ij} parameters) calculated for the segregated I-Exp from sample B.

B-AD	I 9.98 Å	Exp1 15.00 Å	Exp2 12.50 Å
I 9.98 Å	0.465	0.116	0.069
Exp1 15.00 Å	0.109	0.074	0.027
Exp2 12.50 Å	0.075	0.021	0.044

B-EG	I 9.98 Å	Exp1 16.76 Å	Exp2 14.00 Å
I 9.98 Å	0.465	0.140	0.044
Exp1 16.76 Å	0.140	0.130	0.000
Exp2 14.00 Å	0.044	0.000	0.036

B	I	Exp1	Exp'	Exp2
I	0.465	0.116	0.025	0.044
Exp1	0.109	0.074	0.027	0.000
Exp'	0.031	0.021	0.008	0.000
Exp2	0.044	0.000	0.000	0.036

Note: The W_{ij} matrices obtained for AD and EG states are equivalent if Exp layers from the present table are combined as follows: $Exp1_{AD}$ = Exp1, $Exp2_{AD}$ = Exp' + Exp2, $Exp1_{EG}$ = Exp1 + Exp', and $Exp2_{EG}$ = Exp2.

Table A-1C. Single-phase segregated I-Exp model. Relative abundance of the different layer pairs (W_{ij} parameters) calculated for the segregated I-Exp from sample C.

C-AD	I 9.98 Å	Exp1 15.00 Å	Exp2 12.50 Å
I 9.98 Å	0.445	0.090	0.116
Exp1 14.90 Å	0.090	0.023	0.038
Exp2 12.50 Å	0.116	0.048	0.036

C-EG	I 9.98 Å	Exp1 16.76 Å	Exp2 14.00 Å
I 9.98 Å	0.444	0.162	0.044
Exp1 16.76 Å	0.162	0.108	0.000
Exp2 14.00 Å	0.044	0.000	0.036

C	I	Exp1	Exp'	Exp2
I	0.445	0.090	0.072	0.044
Exp1	0.090	0.023	0.038	0.000
Exp'	0.072	0.048	0.000	0.000
Exp2	0.044	0.000	0.000	0.036

Note: The W_{ij} matrices obtained for AD and EG states are equivalent if Exp layers from the present table are combined as follows: $Exp1_{AD}$ = Exp1, $Exp2_{AD}$ = Exp' + Exp2, $Exp1_{EG}$ = Exp1 + Exp', and $Exp2_{EG}$ = Exp2.

Table A-2. Relative abundance of layers, layer pairs and triplets determined for the hypothesized solid-state transformation transition between the I-Exp phase from sample C and the I-Exp-Ch phase from sample D.

	Samples									
Layer Sequence	Sample C W_{XRD}		Inter. phase I W_{Cal}	Inter. phase I W_{XRD}		Inter. phase II W_{Cal}	Inter. phase II W_{XRD}		Sample D W_{Cal}	Sample D W_{XRD}
I	0.67		0.68	0.68		0.69	0.69		0.70	0.70
Exp	0.33	→	0.27	0.27	→	0.21	0.21	→	0.15	0.15
Ch	0.00		0.05	0.05		0.10	0.10		0.15	0.15
II	0.4489		0.4684	0.4684		0.4879	0.4878		0.5072	0.5072
IExp	0.2211	→	0.1798	0.1798	→	0.1413	0.1413	→	0.1050	0.1050
ICh	0.0000		0.0319	0.0319		0.0609	0.0609		0.0878	0.0878
ExpI	0.2211	→	0.1836	0.1836	→	0.1449	0.1449	→	0.1050	0.1050
ExpExp	0.1089	→	0.0729	0.0729	→	0.0441	0.0441	→	0.0225	0.0225
ExpCh	0.0000		0.0135	0.0135		0.0210	0.0210		0.0225	0.0225
ChI	0.000		0.0280	0.0280		0.0573	0.0573		0.0878	0.0878
ChExp	0.000		0.0173	0.0173		0.0246	0.0246	→	0.0225	0.0225
ChCh	0.000		0.0046	0.0046		0.0181	0.0181		0.0397	0.0398
III	0.3008		0.3200	0.3226		0.3424	0.3449		0.3647	0.3676
IIExp	0.1481	→	0.1241	0.1238	→	0.1007	0.0999	→	0.0768	0.0761
IICh	0.0000		0.0214	0.0219		0.0419	0.0430		0.0621	0.0636
IExpI	0.1481	→	0.1217	0.1223	→	0.0958	0.0975	→	0.0716	0.0735
IExpExp	0.0730	→	0.0559	0.0485	→	0.0356	0.0297	→	0.0204	0.0158
IExpC	0.0000		0.0030	0.0090		0.0104	0.0141		0.0143	0.0158
IChI	0.0000		0.0201	0.0179		0.0374	0.0349		0.0545	0.0513
IChExp	0.0000		0.0109	0.0110		0.0180	0.0150	→	0.0180	0.0132
IChCh	0.0000		0.0010	0.0030		0.0056	0.0110		0.0154	0.0233
ExpII	0.1481	→	0.1267	0.1265	→	0.1032	0.1024	→	0.0768	0.0761
ExpIExp	0.0730	→	0.0600	0.0485	→	0.0382	0.0297	→	0.0218	0.0158
ExpICh	0.0000		0.0053	0.0086		0.0125	0.0128		0.0156	0.0132
ExpExpI	0.0730	→	0.0567	0.0496	→	0.0365	0.0304	→	0.0205	0.0158
ExpExpExp	0.0359	→	0.0240	0.0197	→	0.0120	0.0093	→	0.0048	0.0034
ExpExpCh	0.0000		0.0022	0.0036		0.0046	0.0044	→	0.0024	0.0034
ExpChI	0.0000		0.0091	0.0076		0.0147	0.0120		0.0169	0.0132
ExpChExp	0.0000		0.0051	0.0047		0.0067	0.0052	→	0.0050	0.0034
ExpChCh	0.0000		0.0008	0.0013		0.0031	0.0038		0.0064	0.0060
ChII	0.0000		0.0188	0.0193		0.0395	0.0405		0.0630	0.0636
ChIExp	0.0000		0.0046	0.0074		0.0113	0.0117		0.0149	0.0132
ChICh	0.0000		0.0000	0.0013		0.0013	0.0051		0.0051	0.0110
ChExpI	0.0000		0.0038	0.0118		0.0132	0.0170	→	0.0130	0.0158
ChExpExp	0.0000		0.0029	0.0047		0.0057	0.0052	→	0.0034	0.0034
ChExpCh	0.0000		0.0000	0.0009		0.0009	0.0025		0.0026	0.0034
ChChI	0.0000		0.0010	0.0026		0.0052	0.0104		0.0168	0.0233
ChChExp	0.0000		0.0008	0.0016		0.0034	0.0045		0.0068	0.0060
ChChCh	0.0000		0.0000	0.0004		0.0004	0.0033		0.0068	0.0105

Note: W_{XRD} values are deduced directly from the structure model determined from I-Exp in sample C and for I-Exp-Ch in sample D. For the theoretical phase I and II, W_{XRD} values are deduced from the hypothesized structure models intermediate between the two end-members (see text for details). W_{Cal} values are calculated assuming the redistribution of layers, layer pairs and triplets whose relative proportion is decreasing from one step to the next one. These layers, layer pairs and triplets are indicated by arrows in the present table. Redistribution of these layers, layer pairs and triplets is described in table A-3.

Table A-3A. Redistribution of layer pairs whose relative proportion is decreasing from one step to the next one during the hypothesized solid-state transformation transition between the I-Exp phase in sample C and the I-Exp-Ch phase in sample D.

I-Exp in sample C		Phase I	
0.2211	IExp	II	0.0094
		IExp	0.1798
		ICh	0.0319
0.2211	ExpI	II	0.0095
		ExpI	0.1836
		ChI	0.0280
0.1089	ExpExp	II	0.0006
		ExpCh	0.0135
		ExpExp	0.0729
		ChExp	0.0173
		ChCh	0.0046

Note: Layer pairs whose proportion is stable or increasing during any of the three steps are not reported in the present table. Their relative abundances, reported in table A-2, are calculated as the sum of their relative abundance in the previous reaction step and of the present redistribution.

Phase I		Phase II	
0.1798	IExp	II	0.0095
		IExp	0.1413
		ICh	0.0290
0.1836	ExpI	II	0.0095
		ExpI	0.1449
		ChI	0.0292
0.0729	ExpExp	II	0.0005
		ExpCh	0.0075
		ExpExp	0.0441
		ChExp	0.0073
		ChCh	0.0135
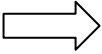
Phase II		⟹ I-Exp-Ch in sample D	
0.1413	IExp	II	0.0094
		IExp	0.1050
		ICh	0.0269
0.1449	ExpI	II	0.0094
		ExpI	0.1050
		ChI	0.0305
0.0441	ExpExp	II	0.0006
		ExpCh	0.0015
		ExpExp	0.0225
		ChCh	0.0195
0.0246	ChExp	ChExp	0.0225
		ChCh	0.0021

Table A-3B. Redistribution of layer triplets whose relative proportion is decreasing from one step to the next one during the hypothesized solid-state transformation transition between the I-Exp phase in sample C and the I-Exp-Ch phase in sample D.

I-Exp in sample C		Phase I	
0.1481	IIExp	III	0.0063
		IIExp	0.1204
		IICh	0.0214
0.1481	IExpI	III	0.0031
		IExpI	0.0602
		IChI	0.0107
		III	0.0032
		IExpI	0.0615
		IChI	0.0094
0.0730	IExpExp	IIExp	0.0021
		IExpExp	0.0398
		IChExp	0.0071
		III	0.0001
		IExpCh	0.0030
		IExpExp	0.0161
		IChExp	0.0038
		IChCh	0.0010
0.1481	ExpII	III	0.0064
		ExpII	0.1230
		ChII	0.0188
0.0730	ExpIExp	IIExp	0.0016
		ExpIExp	0.0303
		ChIExp	0.0046
		ExpII	0.0016
		ExpIExp	0.0297
		ExpICh	0.0053
0.0730	ExpExpI	III	0.0001
		ExpChI	0.0029
		ExpExpI	0.0161
		ChExpI	0.0038
		ChChI	0.0010
		ExpII	0.0021
		ExpExpI	0.0406
		ExpChI	0.0062
0.0359	ExpExpExp	ExpChExp	0.0022
		ExpExpExp	0.0120
		ChExpExp	0.0029
		ChChExp	0.0008
		ExpExpCh	0.0022
		ExpExpExp	0.0120
		ExpChExp	0.0029

66

| | ExpChCh | 0.0008 |

Note: The redistribution of layer triplets among newly formed ones is done assuming that the transition probability from one layer pair to another does not depend on the preceding or following layer as R = 1 (see text for details). Layer triplets whose proportion is stable or increasing during any of the three steps are not reported in the present table. Their relative abundances, reported in table A-2, are calculated as the sum of their relative abundance in the previous reaction step and of the present redistribution.

Table A-3B continued

Phase I		Phase II	
		III	0.0066
0.1241	IIExp	IIExp	0.0975
		IICh	0.0200
		III	0.0032
		IExpI	0.0473
0.1217	IExpI	IChI	0.0097
		III	0.0032
		IExpI	0.0485
		IChI	0.0098
		IIExp	0.0018
		IExpExp	0.0271
		IChExp	0.0056
0.0485	IExpExp	III	0.0001
		IExpCh	0.0014
		IExpExp	0.0085
		IChExp	0.0014
		IChCh	0.0026
		III	0.0066
0.1267	ExpII	ExpII	0.1000
		ChII	0.0202
		IIExp	0.0013
		ExpIExp	0.0189
		ChIExp	0.0039
0.0485	ExpIExp	ExpII	0.0013
		ExpIExp	0.0193
		ExpICh	0.0039
		III	0.0001
		ExpChI	0.0015
		ExpExpI	0.0085
		ChExpI	0.0014
0.0496	ExpExpI	ChChI	0.0026
		ExpII	0.0018
		ExpExpI	0.0280
		ExpChI	0.0056
		IIExp	0.0001
		ExpChExp	0.0010
		ExpExpExp	0.0060
		ChExpExp	0.0010
		ChChExp	0.0018
0.0197	ExpExpExp	ExpII	0.0001
		ExpExpCh	0.0010
		ExpExpExp	0.0060
		ExpChExp	0.0010
		ExpChCh	0.0018

Table A-3B continued

Phase II			I-Exp-Ch in sample D	
			III	0.0066
0.0999	IIExp		IIExp	0.0742
			IICh	0.0190
			III	0.0032
			IExpI	0.0358
			IChI	0.0092
0.0975	IExpI		III	0.0032
			IExpI	0.0358
			IChI	0.0104
			IIExp	0.0015
			IExpExp	0.0168
			IChExp	0.0043
0.0297	IExpExp		III	0.0001
			IExpCh	0.0002
			IExpExp	0.0036
			IChCh	0.0031
0.0150	IChExp		IChExp	0.0137
			IChCh	0.0013
			III	0.0066
0.1024	ExpII		ExpII	0.0742
			ChII	0.0216
			IIExp	0.0010
			ExpIExp	0.0109
			ChIExp	0.0032
0.0297	ExpIExp		ExpII	0.0010
			ExpIExp	0.0109
			ExpICh	0.0028
			III	0.0001
			ExpExpI	0.0036
			ChExpI	0.0002
0.0304	ExpExpI		ChChI	0.0031
			ExpII	0.0015
			ExpExpI	0.0169
			ExpChI	0.0049
			IIExp	0.0001
			ExpChExp	0.0002
			ExpExpExp	0.0024
			ChChExp	0.0021
0.0093	ExpExpExp		ExpII	0.0001
			ExpExpCh	0.0002
			ExpExpExp	0.0024
			ExpChCh	0.0021

Table A-3B continued

Phase II		I-Exp-Ch in sample D	
0.0150	ExpExpCh	IICh	0.0001
		ExpExpCh	0.0022
		ExpChCh	0.0001
		ChChCh	0.0020
0.0052	ExpChExp	ExpChExp	0.0048
		ExpChCh	0.0004
0.0170	ChExpI	ChExpI	0.0023
		ChChI	0.0002
		ChII	0.0009
		ChExpI	0.0105
		ChChI	0.0031
0.0052	ChExpExp	ChExpExp	0.0017
		ChChExp	0.0002
		ChII	0.0000
		ChExpExp	0.0017
		ChExpCh	0.0001
		ChChCh	0.0015

Sediment age (Ma)

Depth (km)

Carter

Mustang Island

% smectite in I-S

Carter

% smectite in I-S

Mustang Island

Depth (km)

Lanson et al. Fig. 2

EG

A - 2170 m / E-2131 m

B - 3660 m / E-2554 m

C - 4000 m / E-2667 m

D - 4640 m / E-3658 m

E - 5010 m / E-3658 m

Position (°2θ CuKα)

Lanson et al. Fig. 3

A
EG

Int.
×6

A - 2170 m

×2

B - 3660 m

C - 4000 m

Position (°2θ CuKα)

Lanson et al. Fig. 4A

B
AD

Int.
×6

×4

A - 2170 m

B - 3660 m

C - 4000 m

Position (°2θ CuKα)

Lanson et al. Fig. 4B

A
EG

Int.
×6

×2

×4

A - 2170 m

B - 3660 m

C - 4000 m

D - 4640 m

E - 5010 m

F - 5180 m

Position (°2θ CuKα)

Lanson et al. Fig. 5A

B
AD

Int.
×6

×4

×2

A - 2170 m

B - 3660 m

C - 4000 m

D - 4640 m

E - 5010 m

0   5   10   15   20   25   30   35   40   45   50
Position (°2θ CuKα)

Lanson et al. Fig. 5B

Lanson et al. Fig. 6

E - 5010 m / EG

E - 5010 m / AD

Int.
×2

E - 5010 m / AD

A

B

C

Position (°2θ CuKα)

Lanson et al. Fig. 7

A

B

Int.
×2

E - 5010 m / AD

C

×3

B - 3660 m / AD

B - 3660 m / AD

Position (°2θ CuKα)

Lanson et al. Fig. 8

AD

14.8 Å
9.98 Å   4.990 Å   3.327 Å   1.996 Å

Int.
×8

A - 2170 m

×4

B - 3660 m

C - 4000 m

D - 4640 m

×3

E - 5010 m

F - 5180 m

11.6 Å

Position (°2θ CuKα)

A
EG

Int.
×2

B - 3660 m
smectite

I-Exp

K-Exp

illite

kaolinite

chlorite

Position (°2θ CuKα)

B
AD

Int. ×4

B - 3660 m
smectite

I-Exp

K-Exp

illite

kaolinite

chlorite

Position (°2θ CuKα)

Lanson et al. Fig. A-2B

A
EG

E - 5010 m

I-Exp-Ch

I-Exp

K-Exp

illite

kaolinite

chlorite

Position (°2θ CuKα)

B
AD

Int.
×2

E - 5010 m
I-Exp-Ch

I-Exp

K-Exp

illite

kaolinite

chlorite

Position (°2θ CuKα)

Lanson et al. Fig. A-3B

A

B

Int.
×2

E - 5010 m / AD

I-Exp-Ch

I-Exp

0   5   10   15   20   25   30   35   40   45   50

Position (°2θ CuKα)

Lanson et al. Fig. A-4